Applied Materials Today 23 (2021) 101040

Contents lists available at ScienceDirect

Applied Materials Today

journal homepage: www.elsevier.com/locate/apmt

# Prospects for laser based powder bed fusion in the manufacturing of metal electrodes: A review

Patricia Nyamekye[a,*], Pinja Nieminen[b], Mohammad Reza Bilesan[b], Eveliina Repo[b], Heidi Piili[a], Antti Salminen[c]

[a] Research Group of Laser Material Processing, Department of Mechanical Engineering, LUT School of Engineering Scienc, Lappeenranta-Lahti University of Technology, Lappeenranta, FI 53851 Finland
[b] Department of Separation Science, LUT School of Engineering Science, Lappeenranta-Lahti University of Technology, Lappeenranta, Lappeenranta, FI 53850, Finland
[c] Department of Mechanical and Materials Engineering, University of Turku, Turku, FI 20500, Finland

ARTICLE INFO

*Article history:*
Received 12 January 2021
Revised 11 March 2021
Accepted 7 April 2021

*Keywords:*
Electrochemical process
Electrode
Flow optimization
Gold recovery
Laser powder bed fusion

ABSTRACT

Additive manufacturing, (AM), includes seven subcategories that can directly manufacture components structures from a computer-designed model layer by layer. Laser-based powder bed fusion (L-PBF) is one of type of the subcategories of AM. L-PBF is a fast and cost-efficient production method that offers the advantages of being implementable with a diverse range of raw materials, possessing a high level of freedom in customization, and producing less waste. L-PBF can potentially enable the production of hierarchically complex shaped electrochemical separation units. This study examines the use of L-PBF for the fabrication of metal electrodes for electrochemical processes. The aim is to address a literature gap by presenting a state-of-the-art review of L-PBF electrodes used in electrochemical cells. The study investigates existing research on electrochemistry and identifies potential benefits from use of L-PBF metal electrodes. Electrochemical reactors in industry require electrodes with a large electrode/electrolyte interface that can hold electrolytes efficiently and reduce the diffusion path of electrons and ions on the active surface of electrode. Meeting these demands require electrodes with specific characteristics such as high surface area and improved mass transport. This review shows that L-PBF can manufacture optimized electrodes satisfying the requirements for electrochemical cells in industrial applications



## 1. Introduction

Additive manufacturing (AM), popularly known as 3D printing, is defined as the "process of joining materials to make parts from 3D model data, usually layer upon layer, as opposed to subtractive manufacturing and formative manufacturing methodologies" [1]. The 3D model refers to computer-aided design (CAD) models, which are either designed from sketches or generated from scans of exiting objects. Scanning of component geometry to a CAD model is often used in reverse engineering, where 3D laser scanners can be used to obtain outer geometries. Inner features of the product are, however, not detected by this method [2–4].

AM methods are divided into seven subcategories, according to ISO/ASTM 52900-2015 [1]. In its category, powder bed fusion (PBF) is defined as a "*process in which thermal energy selectively fuses regions of a powder bed*" [1]. Thus, powder bed fusion refers to AM systems with a building area where raw materials in powder form are laid for melting [1,5]. PBF is further grouped into two subcategories according to the energy source, namely, laser-based powder bed fusion (L-PBF) and electron beam-based powder bed fusion (E-PBF) [6]. The two PBF methods differ in terms of the parts, type of heat source, resolution, process layout, need for a vacuum in the chamber, and melting mechanism of the powder.

Recent studies have indicated that the emerging metal AM method of L-PBF is gaining acceptance in biomaterial engineering and industrial engineering. L-PBF finds usage in the electronics, automobile, aerospace, and petrochemical industries [7–15]. Furthermore, L-PBF manufacturing has attracted attention in the last decade in research institutes and industrial companies as a frontier to the digital revolution, termed Industry 4.0 [7–13]. The technique is predicted to become a viable option to conventional manufacturing in cases where lightweight, complexity, and cus-

* Corresponding author.
*E-mail address:* patricia.nyamekye@lut.fi (P. Nyamekye).

https://doi.org/10.1016/j.apmt.2021.101040

tomization are beneficial [16–18]. L-PBF offers new opportunities to multi material macro/micro metal components, potential option to cost-effective, complex component and customization production [19,20]. Medical field is one sector using L-PBF and multi material to create unprecedented designs to meet specific needs of patients [21]. The integration of L-PBF and new range of functional materials is a viable means to create high value components which require lightweight and customized designs to leverage cost [22,23]. New emerging functional material offer new ways of hybrid manufacturing of multi-material [24], multi-body design [25] and or multi-manufacturing method [26,27] to overcome some of the existing limitations in manufacturing systems. For example, multi-materials and consolidated designs can improve performance by creating components of improved homogeneity with seamless joints and characteristics. This reduce risk of joint leakage and thermal bridges in applications where joints may affect performance [28,29]. Electrodes are components whose optimal performance benefits from complex geometries and customization, making L-PBF a promising alternative for electrodes production [30,31]. In this article, electrodes made from metal materials and L-PBF are presented. The review highlights some of the benefits L-PBF, offer to electrochemical separation processes. L-PBF can build electrodes of varying structural composition, surface roughness, geometry, orientation, and electrocatalytic activity, [30,32]. Consequently, controlling and tuning electrode performance can suit different conditions and applications [30,31,33].

### 1.1. Laser-based powder bed fusion

The first steps for producing parts with L-PBF comprise of idea creation, definition of functions, requirements, and restrictions, and designing and planning the sketches (or scanning) followed by CAD modeling of the desired products. In this initial phase, support structures are also added to the actual workpiece. The next step is converting the CAD model to a readable STL file format appropriate for specific construction machines where required. STL files describe only the triangulated surface geometry of 3D object without any color representation. In other words, STL conversion means the conversion of a solid digital model into a digital model triangulated surface model. Conversion to STL format is done in order to reduce the file size. The STL file is then sliced with special software to acquire the layer-by-layer readable G-codes data needed to print components on the machine system [34]. The L-PBF machine fabricates the physical components based on this sliced data. Machine set-up is done, together with slicing, following necessary modification, and selecting suitable process parameters before the actual building. The building of components follows layer by layer until the entire model is completed [35]. The powder is then removed, and the part is taken out of the building chamber with the building platform. The finished product is removed from the platform and supports before the part undergoes any required post-processing. **Fig. 1** shows the process steps and the equipment layout in L-PBF manufacturing.

### 1.2. Electrochemical processes

In electrochemical processes, oxidation–reduction reactions occur as charged ions either gain or lose electrons, which creates an electric current [37–39]. An electrode can act as an electron donor (cathode) or an electron acceptor (anode) [37]. In electrochemical contexts, an electrode can be defined as a half-cell between one or more ionic conductors and an electron conductor. Thus, electrodes are the combination of an electronically conducting material in contact with an ionically conducting phase. The half-cell consists

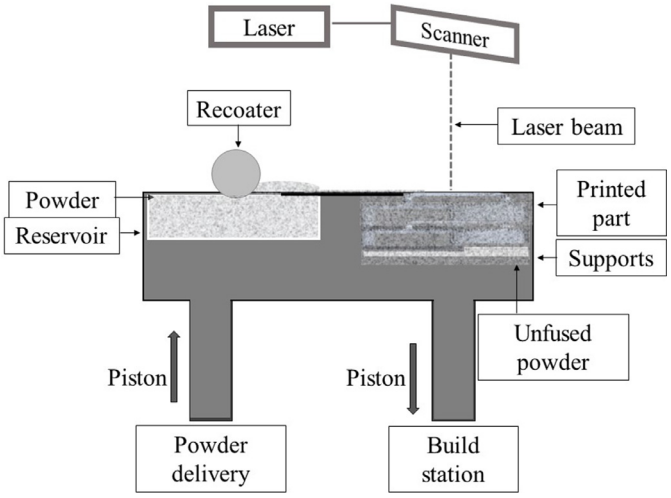


**Fig. 1.** Schematic of A) steps of L-PBF process, and B) layout of principle of L-PBF adapted from [36].

of at least one electron conductor and at least one ionic conductor (electrolyte) [40].

Material transport in electrochemical cells is achieved when fluid transfers electricity by flowing through a porous medium under the influence of a uniform magnetic field. The flow velocity, appropriate catalyst, and the high surface area of the electrode can increase the reactions at the surface of the electrodes. Recent advances in modeling and scaling two-phase solid particle/liquid electrolyte systems brought new research principles on chemical and electrochemical [41]. Additionally, researchers evaluated simultaneous mass transfer and chemical reactions. The combined effects of heat and mass transfer on Magnetohydrodynamics (MHD) flow of a water-based nanofluid form in a porous medium with the different forms of nanoparticles have been studied so far [42,43]. The unsteady flow of a fluid over a vertical plate embedded in a porous medium, with time-dependent velocity, temperature, and concentration, was considered at the different forms of spherical nanoparticles. According to the results, MHD and porosity parameters showed the same effect on surface friction than the velocity parameter. Through a drop in fluid velocity due to the porosity, the surface friction between the particles increases. The surface friction causes the force to prevent the relative motion between the electrolyte and electrode. This resistive force is due to molecular adhesion [42–44]. Based on the conclusions, as the fluid velocity decreases, the thermal boundary layer thickness and the concentration gradient close to the electrode decrease [45]. Besides, due to the drop in the fluid velocity and the concentration level, the chemical reaction parameter could be increased. In another word, as the chemical reaction parameter increases the fluid velocity as well as the concentration level decreases [46].

Combining porous L-PBF electrodes and flow reactors allows to create high-efficiency hybrid tubular cells with thin-film electrolytes for rapid generation of in situ oxidants for fast indirect electrosynthesis. Materials for electronic conductors include pure metals, metal oxides, carbon, and various alloys. Applications of electrodes include electrochemical machining (ECM), electrical discharge machining (EDM), detection of specific substances, water splitting, and rechargeable batteries (REBs) [13,32,47–51]. The steps of electrode manufacturing using L-PBF and areas of application are shown in **Fig. 2.**

The arrows in **Fig. 2** indicate directions of activity. The performance of electrodes can be improved by functional surface modification [37] as shown in **Fig. 2**.

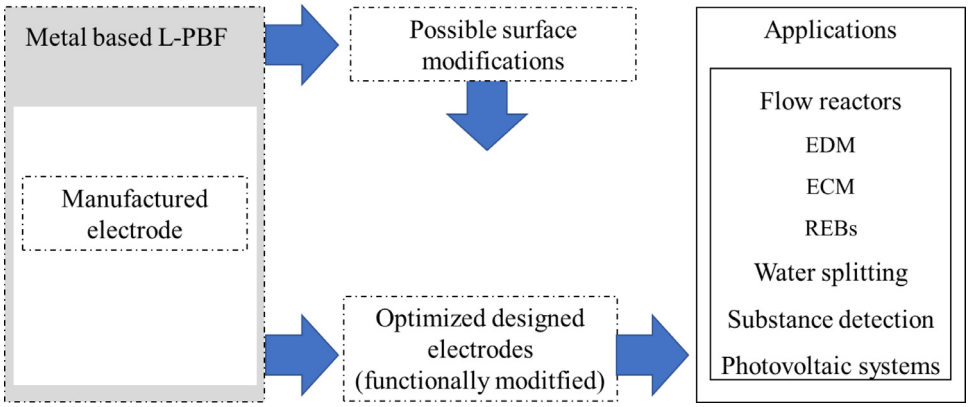


**Fig. 2.** Schematic of electrode manufacturing routes and application fields.

### *1.3. Aims of study*

The use of AM in modern-day manufacturing offers design flexibility and material, energy, and cost efficiencies. The design flexibility offered by AM allows the design of complex and dimensionally accurate components to suit the specific needs of a diverse range of industrial applications [52,53]. Nevertheless, most existing studies have concentrated on AM to improve durability, performance, function, productivity, and esthetic aspects in industries such as the automotive, aerospace, and medical sectors [14,15,54–56]. There also seems to be a lack of published work looking at the specific issue of metal AM electrodes. This study partly addresses this research gap by reviewing research studies related to the AM of metal electrodes used in electrochemical processes. The work considers the potential benefits of using L-PBF in this field.

### *1.4. Methodology*

This research is a comprehensive review of the state-of-the-art of AM/L-PBF for metal electrodes. The study uses the following scientific databases as sources for the literature reviewed: SCOPUS, Google Scholar, ACS Publications, Science Direct, and SpringerLink. The bibliographic search was conducted for the period 2005 to August 2020. The literature review used the following search terms:

1 Additive manufacturing * electrodes (include also studies done with the term “3D printing”)
2 “Powder bed fusion” AND electrodes IN electrochemistry (include also studies done with the term “3D printing”)
3 “Powder bed fusion” AND electrodes IN electrochemistry
4 “Laser powder bed fusion” AND “metal electrodes” IN “powder bed fusion”
5 Additive manufacturing * electrodes * electrochemistry
6 “Laser powder bed fusion” AND “metal electrode” AND electrochemistry

**Fig. 3** shows the number of published articles related to AM and L-PBF for electrochemical electrodes classified according to Google Scholar, ACS Publications, Science Direct, and SpringerLink databases. The trend of yearly publication (only SCOPUS) is given in Fig. 4. The majority of the search results may be a combination of the same topics. For example, results for the search for “Powder bed fusion and electrodes in electrochemistry” were represented for different search term. found with the search for “Laser powder bed fusion and electrodes in electrochemistry”. Specific topics relating to metal-based electrodes with L-PBF were extracted from the search list to suit this study.

As **Fig. 4** shows, AM electrode studies have constantly grown since 2012, and specific studies on AM electrodes for electrochemistry began in 2015. The share of L-PBF of the review shows fewer studies on this topic relative to the total number of studies on AM for electrode applications from 2005 to the present. Many of the existing literature do not separate L-PBF for metal electrodes but rather has been treated as a part of generalized AM/electrode studies. Existing literature often categories such studies with the general term, AM; thus, the research result showing that AM for electrode manufacturing may include other L-PBF. The review includes studies published with “selective laser sintering,” a historical term for L-PBF. The authors assumed, based on random scanning, that many existing studies investigated plastic-based electrodes.

## 2. Design optimization of L-PBF for electrodes

L-PBF can be used to manufacture intricate and complex geometries from metal powder. The possibility of incorporating conformal flow channels within solid bodies, creating lattice frameworks and tortuous channels, and combining multiple parts into a single part can potentially enhance the performance and stability of electrodes [21,40,41]. This, permits several design optimizations in electrochemical applications [21,42,43].

The use of electrodes in flow reactions offers a practical approach to overcome mass transfer limitations employing higher surface area and confinement of the flow in micron or sub-micron sized pores [30,57]. However, flows through electrodes are opposed by inherent material electrical current resistance or boundary-imposed resistance due to layers and sizes [57]. Pressure-induced limitations in the flow channels can be counterbalanced with superposed basic flow induced by secondary flow patterns [57]. The mitigation can be achieved by increasing velocities using microfluidic devices or sectioning [57]. Microfluid devices diminish continuous boundary formation [57] through form-like media [58] and overcome any pressure-related flow resistance. The effects of flow rate on electrodes are discussed in [57–60].

### *2.1. Lattice and tortuous designs*

The term lattice is interdisciplinary and can have different meanings in different disciplines and offer different benefits in different applications. Lattices can be incorporated into components for either functional reasons or as an esthetic feature. Some benefits of creating a lattice in components include better material usage efficiency, weight savings [8], greater surface area [61], and improved charge capacities [62]. A lattice truss in structural design is an arrangement of interconnected beams converging at a common point. The struts that form lattices are constructed through interlocking pins or rigid bonds. The conversion of solid metal bodies to mimic a form-like structure can tailor specific desired properties

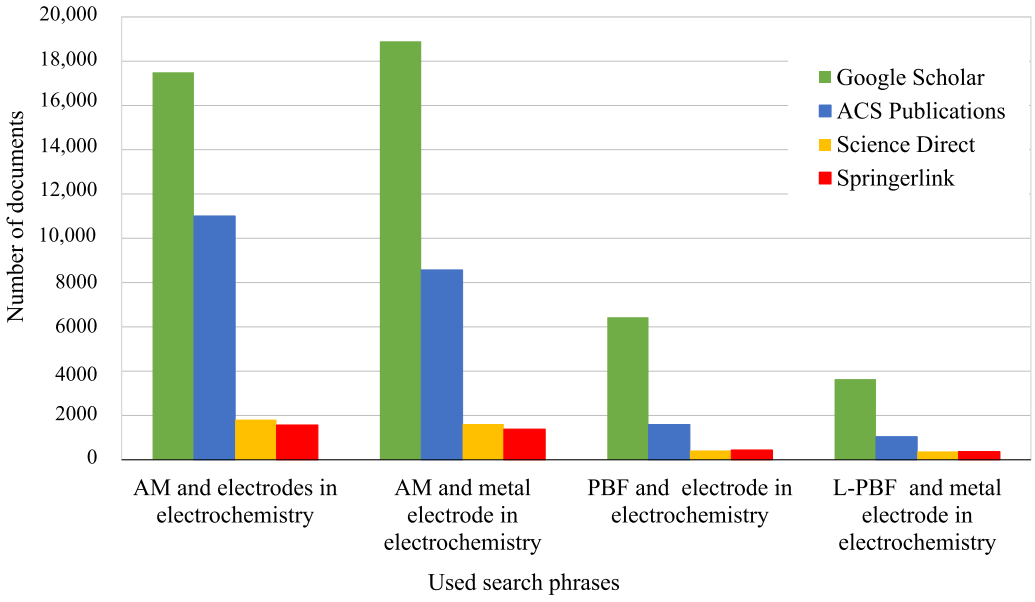


**Fig. 3.** Overview of literatures search results for AM for the databases Google Scholar, ACS Publications, Science Direct and SpringerLink.

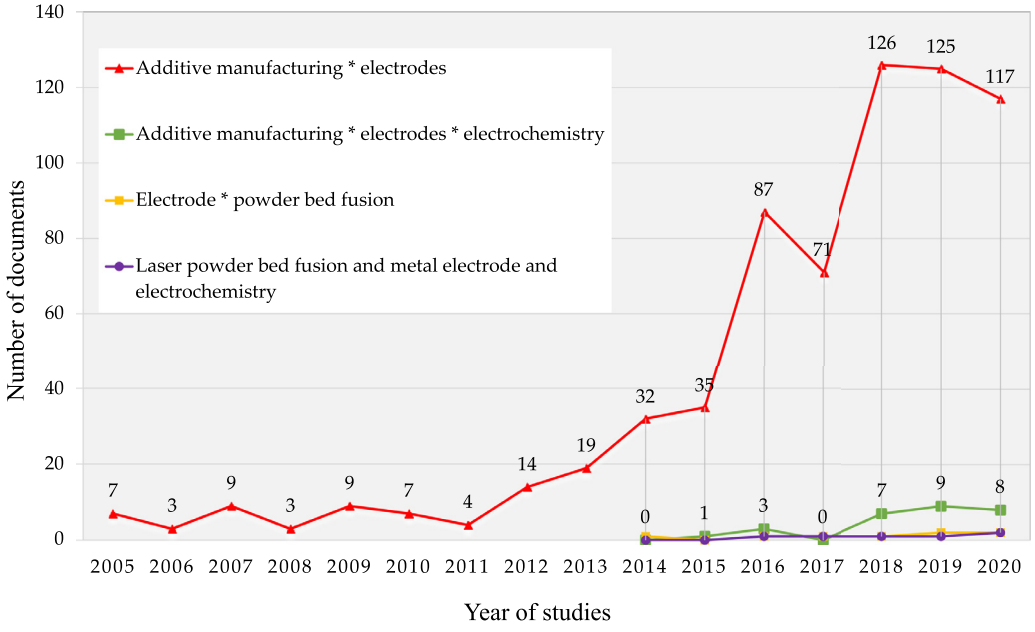


**Fig. 4.** Yearly publication volume of the considered search terms for the SCOPUS database.

such as stiffness, thermal conductivity, electrical resistivity, diffusion, and strength [63,64].

The use of design for additive manufacturing (DfAM) rules and simulation software such as functional generative design and COMSOL Multiphysics can automate the creating of effective and efficient lattices to suit specific flow configurations. The design of intricate structures in fluid flow components with such software is achieved using numerical simulations like finite element analysis (FEA) and computational fluid dynamics (CFD) [32,65]. CFD is a computer-based fluid mechanics tool that can be applied to evaluate fluid flow and related phenomena. FEA is a computer-based tool with which physical phenomena, often phenomena related to structural elements, can be analyzed using numerical methods [66]. Combining fluid flow, structural, and AM simulation can result in optimized lightweight components and better flow conditions [32,67], such as decreasing part weight and pressure drop. Using simulation-driven design allows the isolation and control of specific phenomena. It draws attention to possible ways to alter physical conditions [68] without impairing the performance and functionality of the component [69].

Unlike conventional manufacturing methods, L-PBF uses layer-wise deposition of materials, enabling sophisticated parts of complex shapes [64]. The possibility to manufacture components with little to no shape restrictions makes L-PBF an ideal technique for building components with lattice structures. However, L-PBF is inherently limited in part size and lot size. There is also the possibility of distortions and porosity, which can affect the building process or the reliability of the component. The lattice design needs to be planned such that there is a consideration of possible post-processing methods. The use of support structures for lattices offers more geometric freedom. Complex supports can however increase post-processing time and workload. Due to this rea-

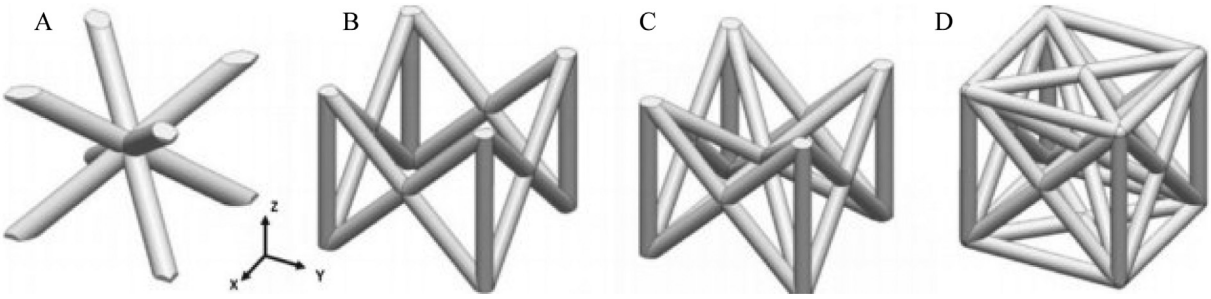


**Fig. 5.** Lattice structure and different configuration of unit cells: A) body centered cubic (BCC), Bb) face centered cubic with vertical struts (FCCZ), C) face and body centered cubic with vertical axis struts (FBCCZ), and D) face and body centered cubic with horizontal and vertical axis struts (FBCCXYZ) [70].

son, self-supporting designs are favoured over inherent overhang angles requiring structural support [70]. Complex geometries must be planned to correlate with the defined building parameters of the specified machine [70]. **Fig. 5** shows examples of configurations of lattice unit cells, arrays of struts, and connections.

As shown in **Fig. 5**, the unit cells of lattice structures can be a combination of different geometries. Each arrangement of cells in **Fig. 5** offers different properties to achieve a desired function. Lattices can be incorporated into metals, polymers, and ceramics of specified cells to define certain shape, size, and thickness [63,71]. L-PBF enables the creating of fully dense lattice-like metal components with tailored biological and mechanical properties [72–74]. Effective control of process parameters must be used to ensure optimal deposition to reduce the forming of undesirable pores. In electrochemical applications, the incorporating a lattice structure has a positive effect on mass transportation, electrical and thermal properties [62,71]. Additionally, the use of lattice-like structured electrodes creates an increased specific mass capacity compared to solid-blocked electrodes. The larger specific mass capacity increases interaction between the electrode and the electrolyte [75].

### 2.2. Fluid flow optimization

Flow in a liquid pipeline may be smooth or laminar flow. Flow turbulence can be altered through higher velocities or flow rates (Reynolds number). Reynolds number (*Re*) is "a *dimensionless number used to categorize the fluids systems in which the effect of viscosity is important in controlling the velocities or the flow pattern of a fluid*" [76]. Relative roughness is "*the amount of surface roughness that exists inside a pipe*" [77]. The roughness has no effect on laminar flow as liquids in laminar flow tend to move with a straight and smooth surface and thus are able to seal off any roughness [78]. The reverse is the case with chaotic flow as *Re* gets higher than 2100 [78]. The effect of roughness can be negligible as *Re* slightly exceeds the critical *Re*-number of 2300. For the reason that laminar sublayers can offset the effect of surface roughness. The transition from laminar to a chaotic state can occur over a range of *Re* [78–80]. Both laminar and turbulent flow can exit at *Re* between 2300 and 4000 [79].

Designing flow channels with segmentation [57] can help increase flow velocity. Creating segments impede the continuous growth depletion boundary which can help overcome the limitations of pressure-driven laminar channel flow by inducing secondary flow patterns[57]. L-PBF can be used to complex segmented features into for electrochemical separation unit with increased surface roughness, e.g., at flow boundaries, which often suffer losses due to flow viscosity. Theoretically, surface roughness decreases frictional and viscous losses in turbulent flows depending on the size and surface of the pipe used [80,81].Increased complexity of flow channel designs with controlled surface roughness and rounded flow joints are some of the benefits that can be obtained from using L-PBF to make metal parts for electrochemical applications. The incorporation of secondary flow into hydraulic applications helps optimize flow dynamics by creating chaotic flow in time and position. Designing flow channels with segmentation, zigzag patterns (see **Fig. 6**A) [82], and rounded flow joints (see **Fig. 6**C) [57, 28] are examples of means to achieve improved flow dynamics.

As can be seen from **Fig. 6**A), *Re* can alter the turbulence of fluid flow [57]. The simulation result in Fig. **Fig. 6**A shows only laminar flow at lower *Re* of 14. At larger *Re*, secondary flows are seen to be present, which intensify as the *Re* number increases. **Fig. 6**B and C show that the configuration of flow in a channel differs based on the sharpness or roundness of the respective inner corners. Traditional manufacturing methods and L-PBF can both manufacture rounded T-shaped pipe designs. The latter is preferred for such designs due to the flexibility and ease to make any shape without intensifying required labor. The flow configuration of metal hydraulic manifolds fabricated with an AM designed arc channel joint in **Fig. 6**C yielded improved efficiencies as follows [28]:

1 Smoother flow transition through a branch with an arc
2 Approximately 78% volume reduction from 535 cm3 to 116 cm3
3 Approximately 35% weight reduction 1.5 kg to 0.98 kg.

Three-dimensional (3D) electrodes including foams and felts can be used in electrochemical reactors to increase the active surface area of the electrode and the efficiency of the system. However, these irregularly shaped electrodes cause tortuosity and channeling effects and impose three to four orders higher pressure drops than would be generated with flat electrodes. AM/L-PBF can effectively manufacture turbulence promotor features with flow guiding structures. Optimizing electrodes with tortuous design can boost turbulence, which can increase velocity and enhance mass transfer without adverse effects on the pressure drop. In addition, L-PBF can be used to manufacture stainless steel electrodes with increased mass transfer coefficient of up to 76% [32] by incorporating complex tortuous flow channels. Tortuous configurations can potentially be used to control the performance of electrodes in, e.g., batteries applications [58]. **Fig. 7** shows three examples of complex-shaped electrode designs achievable with L-PBF, namely, Kenics, Ross low pressure drop (RLPD) and Sulzer mixer electrodes, respectively.

### 2.3. L-PBF and reverse engineering for optimized electrodes

Reverse engineering is an approach to learn from the architecture of an existing component and to use this knowledge to make new improved versions of the part. 3D scanning is one of the quickest ways to convert a physical part to a mesh-like digital format for editing and testing. 3D scanning, however, only gath-

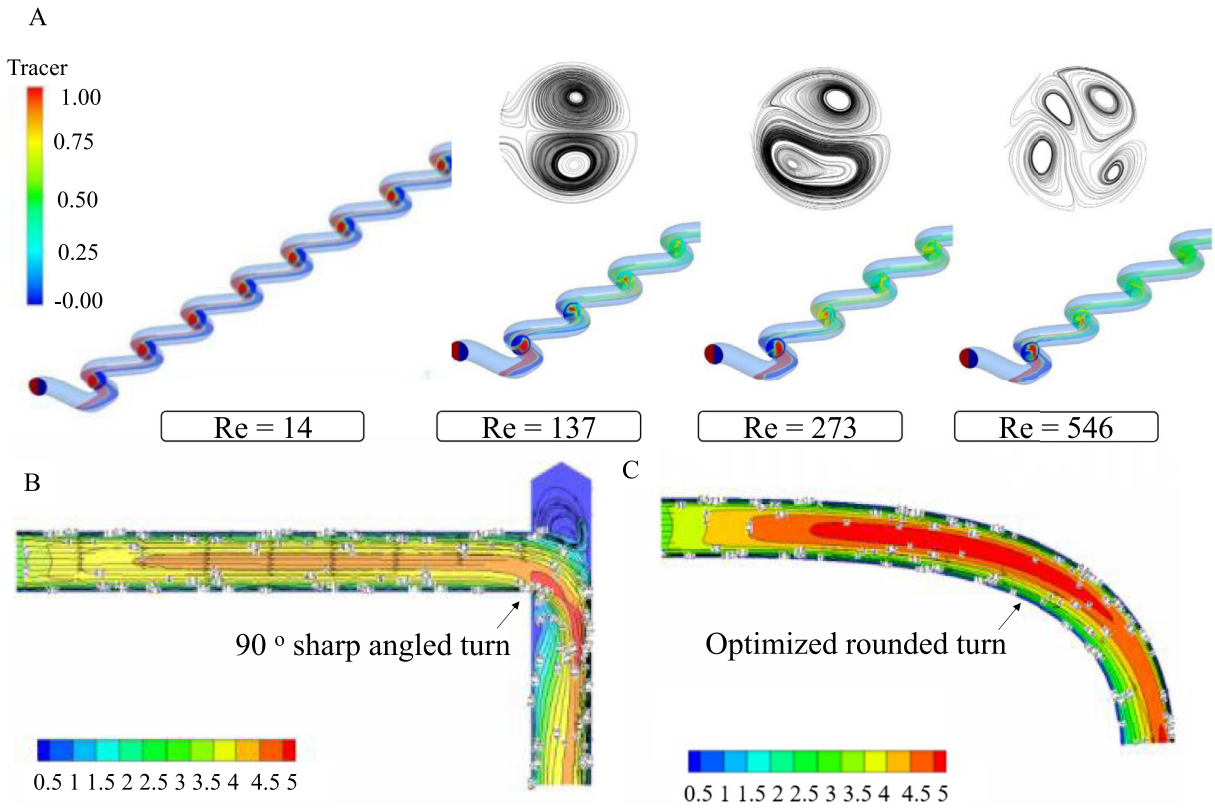


**Fig. 6.** A) Representation of simulated views of the effect of *Re* on zigzag joints channel design flow configuration [57]. An illustration of configuration flow with B) sharp joint and C) rounded joint inner corner designs [28] Fig. 6A) Reproduced with permission from Andre de V., InnoSyn. Fig. 6(B, C) Reproduced with permission from Yi Zhu, Zhejiang University.

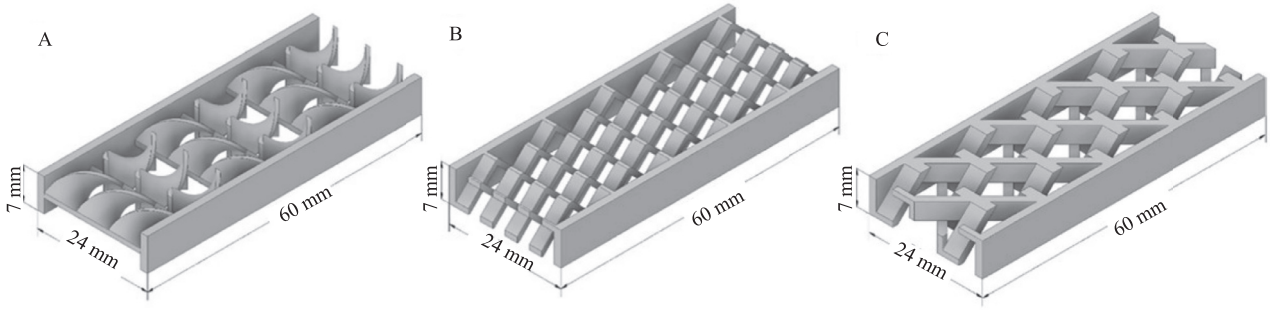


**Fig. 7.** Types of the structured 3D electrodes: (a) Kenics electrode, (b) RLPD electrode and (c) SMX electrode [58].

ers data about the outer surface of the product and does not provide information about complex internal structures. The scanning of complex parts via this contactless technology gives an overall shape and geometry via point cloud data [2,3] and in some simple cases helps to simplify the initial steps of designing and planning.

CAD software tools are used to convert these triangular models to a concise solid model for modification and testing. A robust and cost-effective reconstruction of a new model can be made on demand using rapid AM methods for a prototype or with L-PBF for a functional new part [2,3]. The use of reverse engineering and AM are potentially beneficial for simple designs of electrochemical engineering parts because re-engineering of existing components can easily and affordably be achieved without a need to create and plan new designs. **Fig. 8.** shows an example approach for the use of reverse engineering and AM/L-PBF for existing components (e.g., electrode).

As shown in **Fig. 8**, idea generation is carried out using the skeletal outer geometry of an existing component for new designs, thus reducing the lead time. Laser beam scanning is used to scan, collect, and filter high density cloud point data of the physical part without human interference. These cloud point data are then reconstructed using range images via reverse engineering and specialized software into solid 3D models or reconstructed surface data, as shown in the dotted region in **Fig. 8**. CAD software is a catalyst to this approach. These tools allow a virtual platform to imitate previous designs, detect and modify deficiencies, and simulate, test and perform quality control for redesigned tool parts. The building of the part follows after the design has passed through all stages needed to achieve an optimized electrode design.

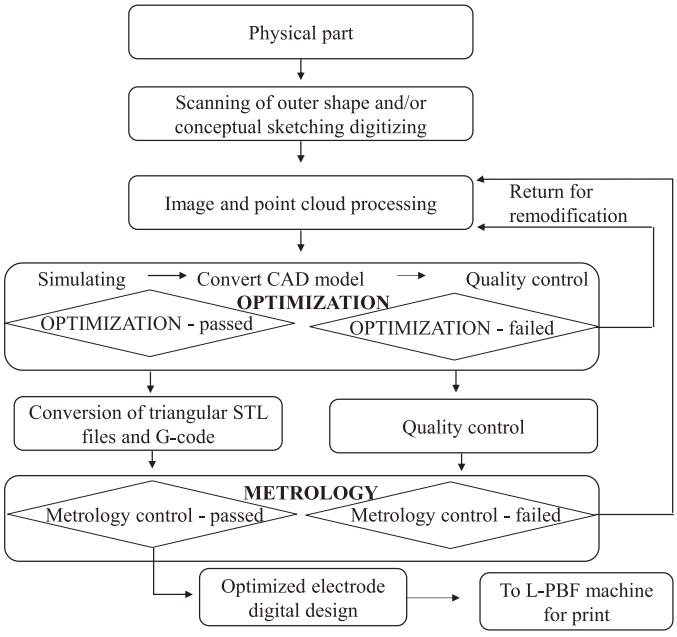


**Fig. 8.** Schematic of reverse engineering and AM to make an optimized electrode for electrochemical applications. Adapted from [2,4,83].

### 2.4. Materials used for L-PBF metal electrodes

When choosing a material and manufacturing process for an electrochemical application, multiple factors need to be considered. The intended application of the component, e.g., an electrode, has to guide selection of the appropriate manufacturing process and materials. Materials with a high melting point and high electrical conductivity properties are sometimes preferred for electrode parts [84]. Examples of materials used for electrochemical applications include stainless steel, aluminum (Al), titanium (Ti), lithium (Li), sodium (Na) and iridium oxide ($IrO_2$). Based on reviewed literature, stainless steel is the most used material for making electrodes. In the reviewed studies, this material is either used as a mixture with other materials or as the base material for the electrodes and coated with other material to improve the electrochemical properties. The use of multi-material electrodes can give combined functionality and improved performance compared with use of a single material. The approach can also result in improved cost-efficiency as well as remove limitations regarding material choice for AM metal electrodes [30,49,85–88]. The base structure of an electrode can be built from easily accessible and cheap material and modified with more expensive or difficult to manufacture material on the surface to suit the application requirements [88,89]. **Fig. 9** lists materials used with L-PBF for electrochemical electrodes and effective coating materials.

**Fig. 9** presents a breakdown of different metal materials used for electrochemical electrodes. Twenty publications out of the total number reviewed were further analyzed for design complexity, material types and related challenges in using L-PBF for electrodes. The review showed that base materials (in blue) were either used singly or bonded with other materials (shown in red) to form multi-material electrodes in order to improve the electrochemical properties. Classification of selected studies into single, multi, and polymer materials printed for electrochemical cells in the cases considered in this review is shown in **Fig. 10.**

As it can be seen from **Fig. 10**, base materials of electrodes in twenty of the reviewed were built as a single material. Five were built with a multiple material. All electrodes built as single material were post processed with other materials to improve electrochemical properties. The two polymer parts shown in yellow were components of the electrode assembly such as housing case which were also manufactured with L-PBF.

## 3. Case studies

Practical usage of metal L-PBF manufactured electrodes in electrochemical applications (devices and processes) are presented in this section.

### 3.1. L-PBF in electrical discharge machining applications

Electrical discharge machining (EDM) is a process for material removal and can be used for machining of materials that have a conductivity of at least 0.01 S/cm [50]. These materials include, for example, ceramics and hardened steels.

Amorim et al. and Sahu and Mahapatra [90] investigated the performances of L-PBF tool electrodes made with pure copper, bronze–nickel alloy, copper/bronze–nickel alloy and steel alloy powders [50] and metal matrix composites of Al, silicon (Si) and magnesium (Mg) (AlSi10Mg) [90] in EDM experiments. The performance of the electrodes was evaluated by material removal rate and volumetric relative wear either with conventionally method [90] or with the different material [50]. Comparatively, the electrodes built with L-PBF from bronze-nickel powder showed the best performance in the EDM process. Overall, the L-PBF manu-

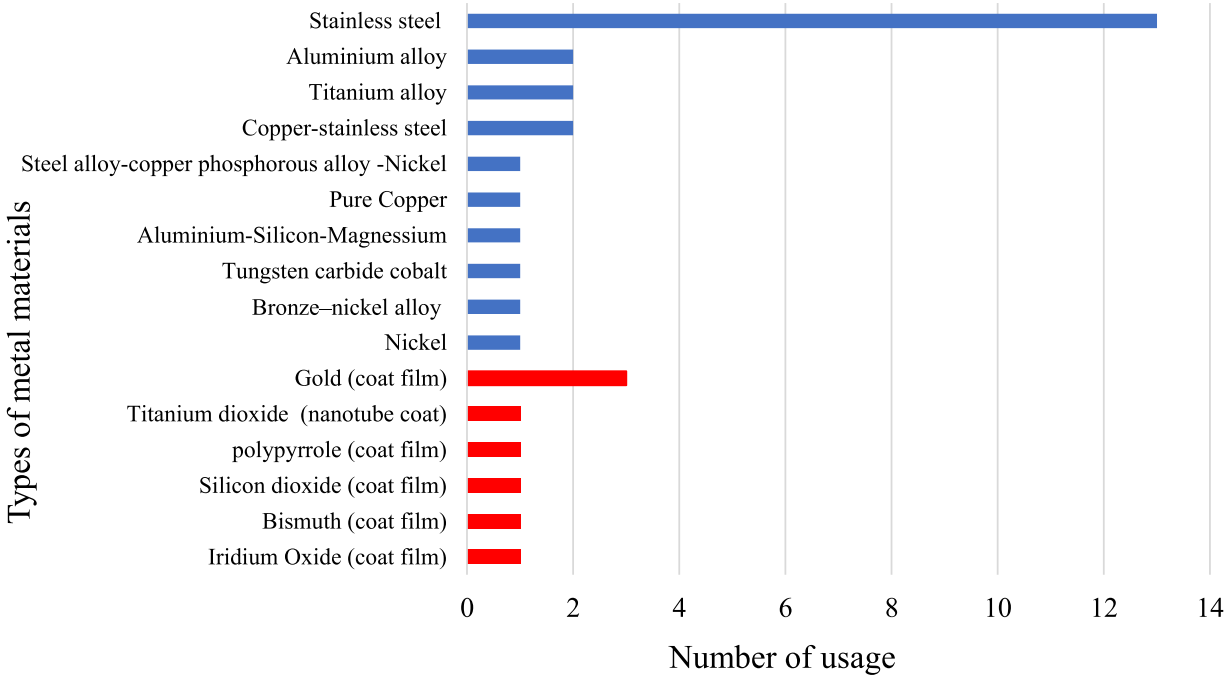


**Fig. 9.** Breakdown of metal materials used for electrochemical electrode applications based on the review.

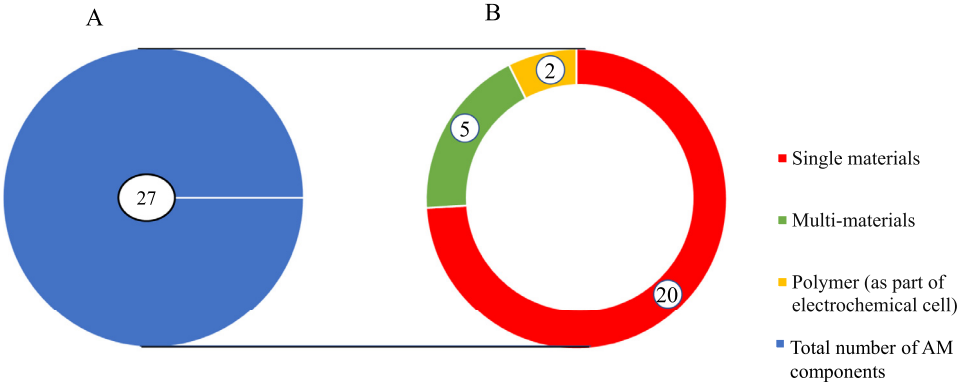


**Fig. 10.** A) Representation of total number of materials reviewed article. B) Overview of material breakdown into specifics.

factured electrodes did not perform as well as comparable solid copper electrodes.

The results presented in [90] show that the use of L-PBF to manufacture tool electrodes for EDM applications can have a positive effect on manufacturing time and costs. The study also shows the suitability of L-PBF for building tool electrodes for EDM. EDX analysis, however, found traces of the tool on the machined material, which the study attributed to insufficient densification of the tool and wear resistance. Further study is required, particularly, as regards development of materials that are suited for both EDM and L-PBF processes. Other areas requiring further investigation include, for instance, optimization of the process parameters to reduce the porosity of the electrodes, improvement in the EDM material removal rate and reduction in the volumetric relative wear [50]. The machine used in the study was an EOS M 250 [50].

Uhlmann *et al.* investigated the performance of a tungsten carbide-cobalt (WC–Co) tool electrode for EDM fabricated with L-PBF and compared its performance with a conventionally manufactured copper E-Cu 58, graphite EX-75, and tungsten carbide CTS20 tool electrode. WC–Co is “an alloy of a hard ceramic phase, the tungsten carbide (WC), and a ductile metallic phase, the cobalt (Co)” [91]. E-Cu 58 (Cu-ETP) [92] is an “oxygen containing copper which has a very high electrical and thermal conductivity” [93]. EX-75 is a graphite-based material developed as "ultra-low consumption finishing for the electrode for applications such as plastic mold making, mold forging, and die casting moulds [94]. CTS20 is a “submicron grain carbide grade for the universal machining of alloyed and non-alloyed steels, titanium alloys and nickel-based alloys” [95]. Conventionally manufactured EDM tool electrodes have limited process conditions, which can be improved with geometrically complex flush channels designed into the tool electrode. Such enhanced conditions create a challenge to conventional methods used to manufacture electrodes. Some of these process limitations might be absent with L-PBF as this method allows flexible manufacturing of complex-shaped geometries. The simultaneous implementation of flushing channels using special materials like tungsten carbide-cobalt might not be as easy with classical manufacturing methods as with L-PBF. The wear resistance of tungsten carbide-cobalt in the EDM process makes it a favourable option [20]. Processing parameters, such as volume energy density (EV) and build direction can be used to alter the final properties of a tool electrode. An example is given in [20], where low EV was used

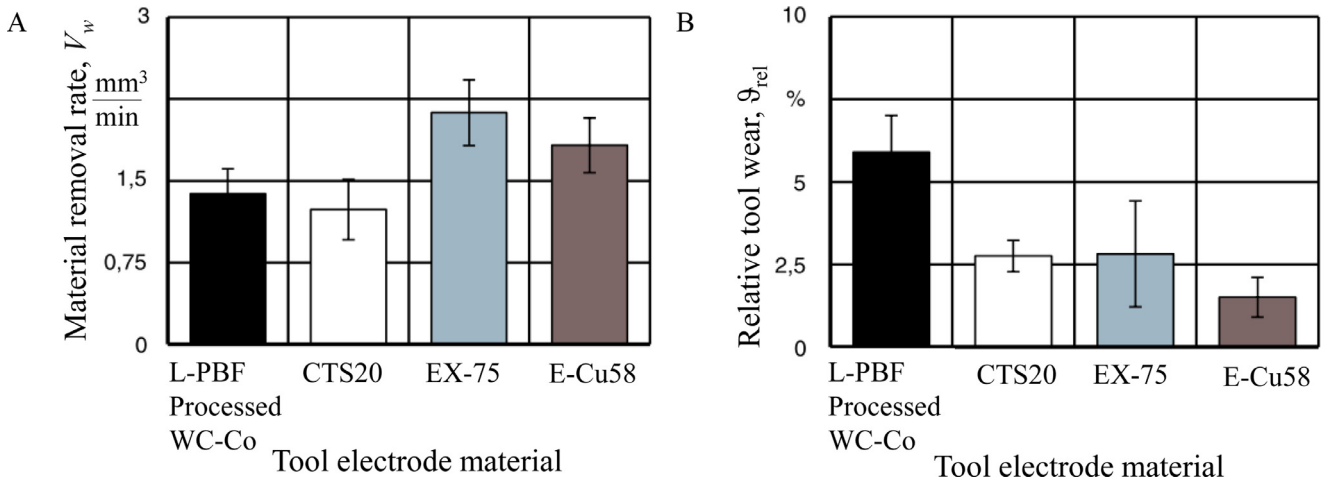


**Fig. 11.** Performance of tool electrodes manufactured with L-PBF and traditional methods. Reproduced with permission from [20]. Copyright 2018 Elsevier.

with high cobalt 12 wt.% tungsten carbide-cobalt, and high EV with low cobalt 3 wt.% tungsten carbide-cobalt. The performances of the electrodes were compared with conventionally manufactured copper E-Cu 58, graphite EX-75, and tungsten carbide CTS20 tool electrodes. A summary of the performance of the electrodes as regards material removal rate (VW) and tool wear ($\vartheta$) is shown in **Fig. 11**.

As seen from **Fig. 11**, the L-PBF electrodes showed the highest relative tool wear of the four electrodes studied in [73]. Using low cobalt content with high $E_V$ resulted in a poor material removal rate, $V_w$ and high tool wear, $\vartheta$, which was due to low electrical conductivity. The performance of the L-PBF electrode was poor when compared with traditional copper E-Cu 58 and graphite EX-75 electrodes. The *Vw* was almost the same for the L-PBF tool electrode and tungsten carbide CTS20 electrode and both electrodes had lower *Vw* than the compared copper E-Cu 58 and graphite EX-75 electrodes. The material removal rate of the L-PBF and CTS 20 electrodes ranged between 1.20–1.35 $mm^3$/min. The main reason for this similarity in poor performance is the low cobalt content, which was almost half the values commonly found in industrial tungsten carbide tube electrodes. The low *Vw* with the L-PBF manufactured electrodes was also attributed to high porosity. Hot Isostatic Pressing (HIP) of both the high and low content tungsten carbide electrodes was done to enhance their performance. HIP increased *Vw* and $\vartheta$ of electrodes built at low *E* with high cobalt content. The post-processing yielded no effect on electrodes built at high $E_V$ with low cobalt content. The study [20] concluded that using appropriate $E_V$ during L-PBF manufacturing and increasing cobalt content can improve the functionality and quantity of the electrodes as these were identified as potential factors that affected the performance of the printed tool electrode. The identified weaknesses highlight aspects that can be optimized to enhance the characteristics of electrodes.

### 3.2. L-PBF in substance detection applications

Ambrosi et al. investigated the manufacturing of customized helical-shaped CL 20ES stainless steel electrodes. The tailored electrodes were designed and manufactured in different sizes to suit a variety of electrochemical applications. The study highlighted the versatility and possibilities offered by L-PBF, such as, customization, complexity, and simultaneous manufacturing of multiple parts. Due to the high charge transfer resistance, the printed stainless steel electrodes were surface modified to suit the applications studied. The stainless steel material exhibited slow electron transfer in alkaline solutions, which makes it a poor material for electrodes intended for such environments. This limitation was solved by depositing an $IrO_2$ film on top of the steel electrode. The functions and properties of the electrodes were characterized by energy dispersive X-ray (EDX) spectroscopy and scanning electrode microscopy. The coated helical electrode showed improved properties such as acting as a pseudocapacitor and evolution catalyst and behaved nernstially as a pH sensor in alkaline solutions **Fig. 12** shows the electrodes designed and voltammograms from the experimental test.

Cheng et al. designed and manufactured a helical stainless steel (iron (Fe) and nickel (Ni) composition) electrode using a Concept Laser machine. The built electrodes were electroplated with gold (Au) for improved electrochemical properties and the performance of the coated electrodes was compared with that of a glassy carbon (GC) electrode. **Fig. 13** shows the CAD model and an optical image of the Au-plated electrode [96].

Elemental mapping analysis of the electrode showed that electroplating can be used effectively to modify the surface functions of stainless steel components by uniform and homogeneous distribution of Au. The electrode designed in the study was used in individual and simultaneous detection of phenol and p-aminophenol (p-AP) using cyclic voltammetry (CV) and differential pulse voltammetry (DPV). Fig. 14 shows a calibration graph of peak current density against phenol and p-AP concentration, respectively.

The results of the study showed that the AM fabricated electrode had higher sensitive and generated intensified signals. The improved sensitivity and signal strength contributed to a higher detection of phenolic compounds. These improvements are due to the efficient electron transfer enabled by the properties of the stainless steel for p-AP detection. However, phenol detection did not show much improvement with the 3D-Au AM built stainless steel electrode as a result of the high rate of adhesion between Au and phenol [96]. Overall, distinct oxidation peaks were observed with the 3D-Au L-PBF electrode. Recommendations to overcome shortcomings that might hinder application of functionally modified AM printed parts as a replacement for conventional electrodes were outlined in the work, one of which is passivation of electrodes used in phenol detention [96].

In a similar study, Lee et al. used L-PBF manufactured electrodes for the detection of heavy metals. Stainless steel was the base material for the designed electrode. The electrochemical properties of the printed electrodes were enhanced by coating the surfaces with either Au or Bismuth (Bi). The modified printed electrodes were applied in individual and simultaneous square wave anodic strip-

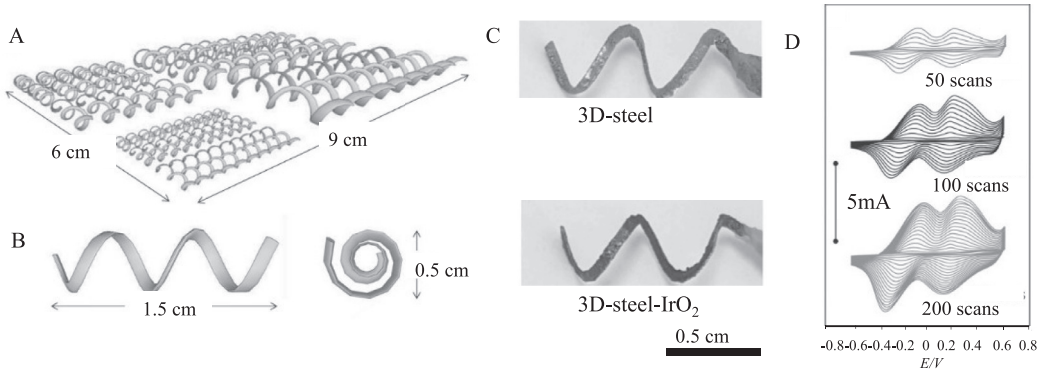


**Fig. 12.** Schematic of A) the designed model, B) closed view of the model, C) printed electrode with $IrO_2$ film coat, and D) cyclic voltammograms after 50, 100 and 200 potential scans [31]. Reproduced with permission from [31]. Copyright 2015 John Wiley & Sons, Inc.

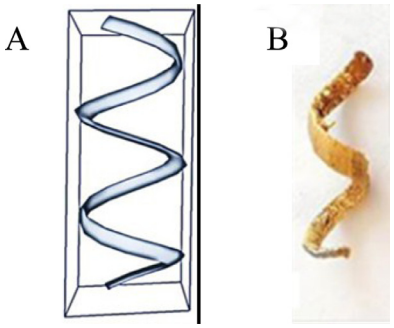


**Fig. 13.** Representation of A) the 3D model and B) optical image of the Au-plated electrode [96]. Redrawn with permission from [96]. Copyright 2017 Elsevier.

ping to analyze lead (Pb) and cadmium (Cd) in an aqueous solution. The study compared the modified printed electrodes with a conventional GC electrode. The designed and printed electrodes used in the study are shown in **Fig. 15.**

A 50–300 ppb concentration of Pb and 50–500 ppb of Cd were used in the experimental study. For the conditions studied, the printed electrodes showed higher sensitivity towards these heavy metals than a conventional GC electrode, as seen in **Fig. 15**E [97]. Improved sensitivity and selectivity of the electrode material towards heavy metals was seen in the 3D-Au and 3D-Bi coated electrodes.

A high-energy laser beam was used to manufacture stainless steel-based electrodes by Liyarita et al. The electrode was helically-shaped and made from stainless steel powder similar to studies [96,97] using a Concept Laser machine. The surface of the printed electrode was modified by coating it with Au. **Fig. 16** shows the CAD model, as-printed stainless steel electrode and the Au-plated electrode [98].

Varying pulse and cyclic voltammetry were utilized for the detection of dopamine and acetaminophen, both individually and simultaneously. The surface of the Au-plated electrode greatly improved peak currents for both acetaminophen and dopamine. In comparison with a conventional GC electrode, the sensitivity of the Au-plated electrode was enhanced three-fold. The sensitivity of the printed electrode was 4.7 times that of a commercial gold disk electrode [98].

### 3.3. L-PBF in an EM application

In the ECM process, the anode electrode is dissolved chemically. When metal ions dissolve, they create hydroxides. Hydrogen is produced in the tool electrode. Koyano et al. used a LUMEX Advance-25 machine to L-PBF manufacture a tool electrode for ECM applications. A multi-material composition of 70 wt.% alloy steel, 20 wt.% copper-phosphorous alloy and 10 wt.% nickel powder printed on a LUMEX Avance-25 machine was used for the electrode. The L-PBF process made it possible to create permeable structures, which influenced the functionality of the electrode tool. Different laser

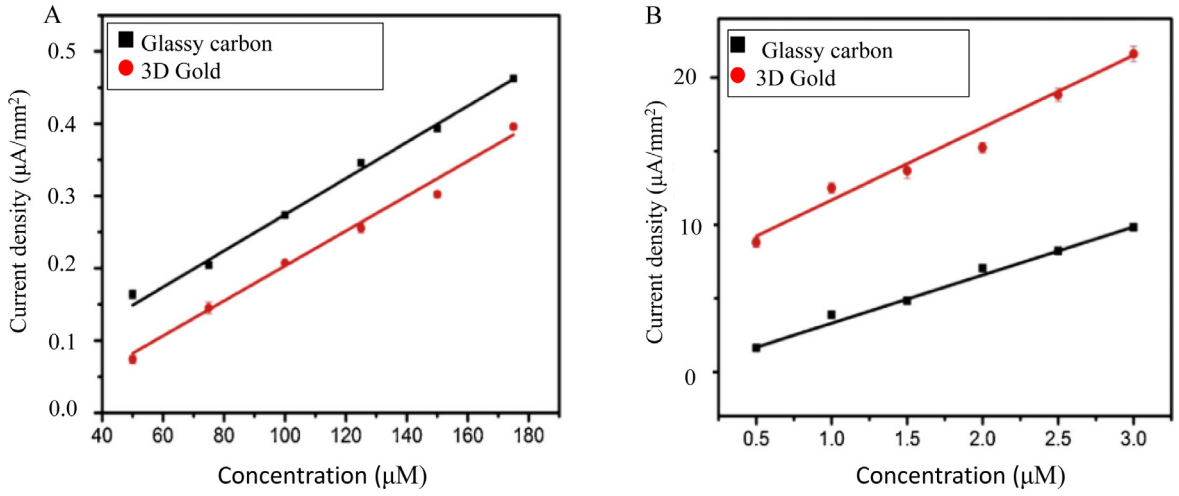


**Fig. 14.** A) Representation of Peak current density against phenol concentration, B) p-AP concentrations [96]. Redrawn with permission from [96]. Copyright 2017 Elsevier.

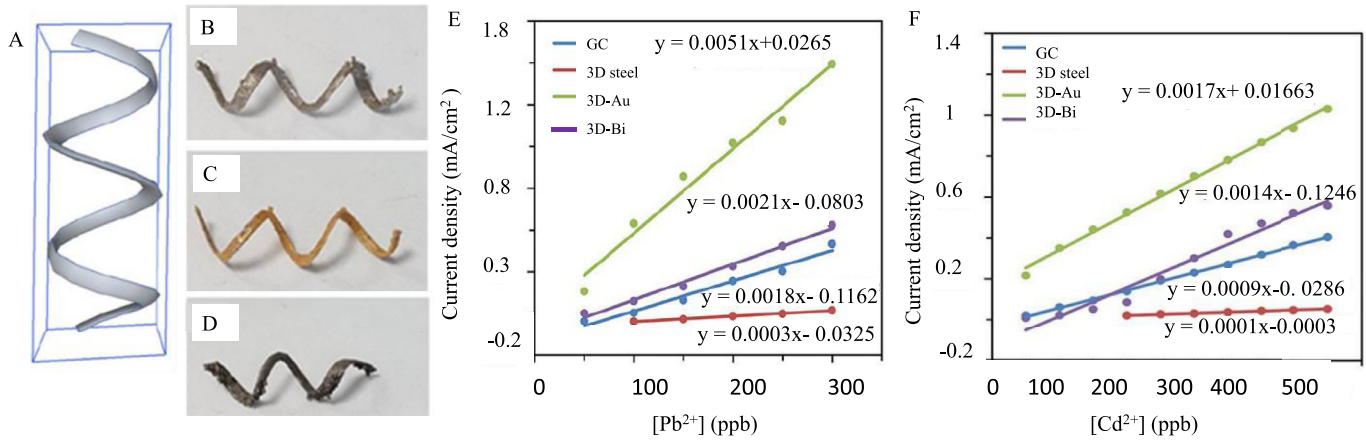


**Fig. 15.** A representation of 3D model of electrode. B) An outlook of the spiral-like printed steel- electrode. C) Representation of the Au-electroplated electrode. D) Bi-electroplated electrode. E) and F) Representations of calibration curve evaluation using current density as a function of Pb and Cd concentrations of comparable electrodes [97]. Modified with permission from [97]. Copyright 2017 John Wiley & Sons, Inc.

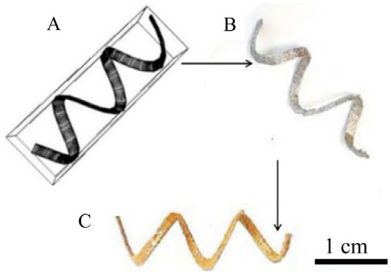


**Fig. 16.** A) Schematic of the 3D model of electrode. B) Illustration of the L-PBF printed stainless steel electrode. C) Representation of the Au-plated electrode [98]. Modified with permission from [98]. Copyright 2018 John Wiley & Sons, Inc.

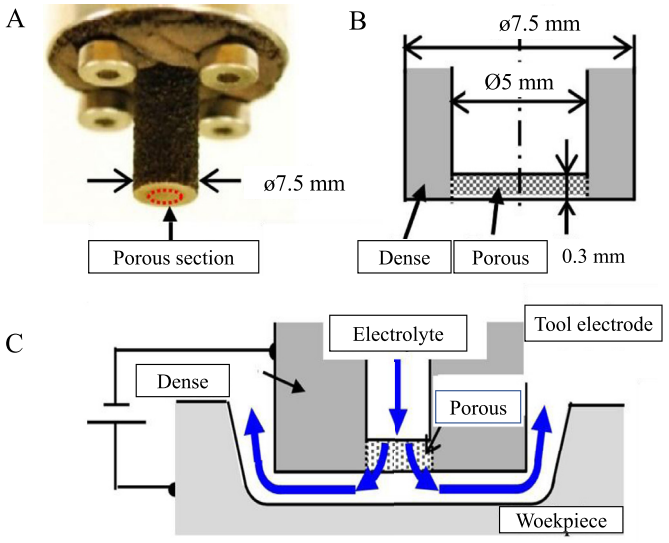


**Fig. 17.** A) Illustration of the general view of electrode design. B) Representation of cross-sectional view of the studied lattice cylindrical electrode. C) Overview of the ECM process arrangement. Adapted with permission from [49]. Copyright 2017 Elsevier.

scanning speeds with a constant laser power resulted in a variety of pore size and porosity. The electrode tool successfully incorporated small pores with large porosity, which was beneficial for improving the flow rate of the electrolyte, and the L-PBF process was able to produce electrodes without protrusions [49]. **Fig. 17** shows the designed electrode and the ECM process set-up utilized in the study.

The study [49] found that the lattice electrode enabled vigorous flow of electrolytic fluid through the permeable structure. The study also highlighted the benefits of alternation of the positioning of the porous structure with a consolidated part. The L-PBF-manufactured electrode had different porosities and tool geometries that would not be possible with conventional manufacturing methods. Although some conventional manufacturing processes, like micro-EDM, can create small pore sizes, L-PBF offers better performance and more cost-effective production for these electrode tools than classical methods.

### 3.4. L-PBF for flow reactors

Arenas et al. used L-PBF (M2 Multilaser machine) to manufacture a lattice electrode for electrochemical flow reactors. The electrode was manufactured with stainless steel. The measurements of the electrode and current collector were 60 mm × 40 × 3.7 mm and 68 × 45 × 2.0 mm, respectively. The electrode structure was designed with an internal and hexagonal grid, as illustrated in **Fig. 18**.

The surface area and porosity of the electrodes improved as a result of the scaffold-like structure generated with L-PBF. The use of L-PBF allowed sufficient control of the as-built electrode to eliminate any excessive thermal deformation or internal porosity, which would have resulted in undesirable flow of moving liquid. The integrated model of the electrode and current collector as a single metal unit can avoid corrosion which would otherwise have occurred at weld joints [30]. The stainless steel electrodes were coated with Ni to enhance their electrochemical properties, which improved the performance of the electrodes. The mass transport characteristics were found to be comparable and even superior to mesh, RVS and conventional planar electrodes.

Lölsberg et al. utilized L-PBF to manufacture a metal electrode and polymer housing of an electrochemical reactor. The aim of their study was to improve the mass transport properties of the electrode and the AM electrode was tested in an electrochemical reactor. Stainless steel (X2CrNiMo 17-12-2) electrodes with helical structures were manufactured on an L-PBF machine. The housing of the reactor was built on a Stratasys Objet Eden 260 V polyjet 3D machine with a material jetting technology utilizing a transparent photopolymeric material (Stratasys, RGD810). The electrodes consisted of repeated unit cells with filaments that were oppositely twisted and connected with a single point. Fig. 19 shows the AM-

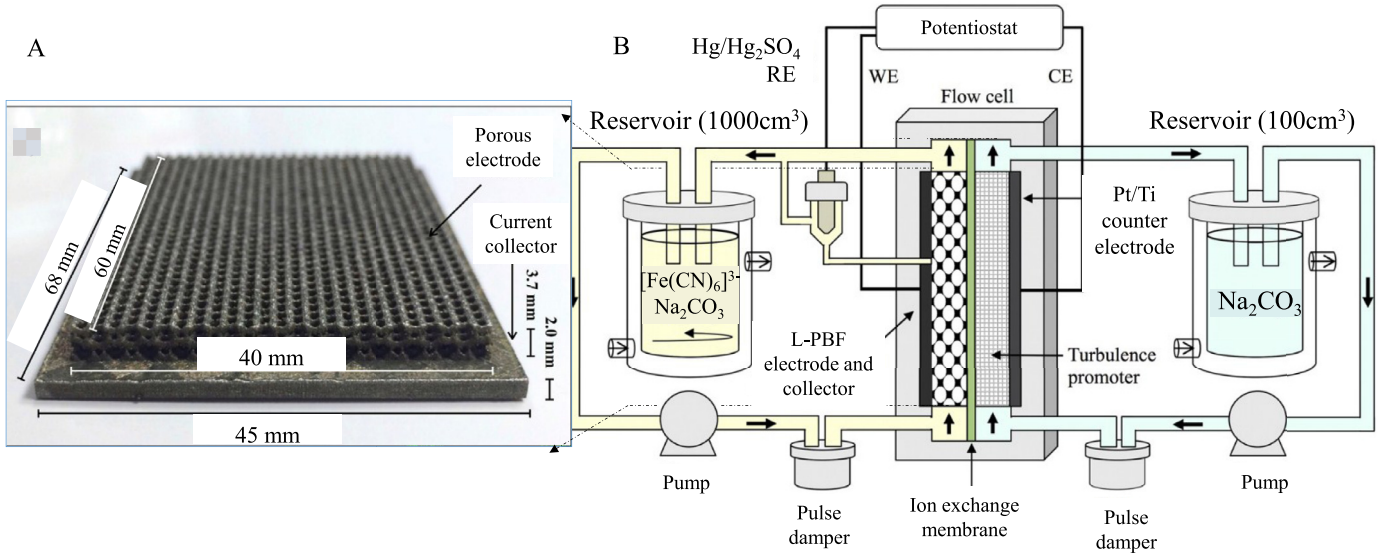


**Fig. 18.** Representation of A) the 3D-printed Ni/SS lattice structure electrode. B) Representation of the experimental set up used in the flow study [30]. Adapted with permission from [30] Copyright 2017 Elsevier.

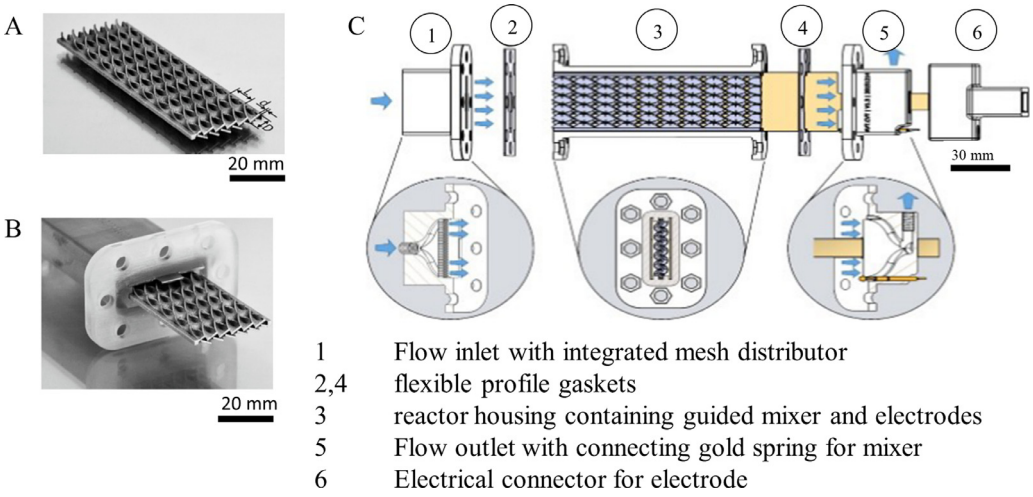


**Fig. 19.** Representation of A) the helical AM electrode mixer, B) cross section showing the electrode mixer, the upper flat electrode reactor cover, and C) the electrochemical reactor, redrawn from [32]. Modified with permission from [32]. Copyright 2017 John Wiley & Sons, Inc.

printed electrode and a schematic of the electrochemical reactor used in this study [32].

The electrochemical flow reactor was tested under specifically defined flow conditions. Simulations of the fluid dynamics started from the design phase. Dead zones and channelling effects could be avoided by including a mesh in the inlet of the channel, thereby optimizing the conditions for homogenous flow distribution. **Fig. 20** shows the flow field inside the electrochemical reactor [32], where **Fig. 20**A shows the inlet when the flow distributor has not been included, **Fig. 20**B when it is in place, and **Fig. 20**C is the unit cell that is repeated along the flow axes shown in **Fig. 20**D [32].

The study highlights the potential of electrodes that allow flow through mixers. The study combined a high surface area and a mixing effect to reduce potential concentration polarization effects caused by stagnation at the electrode-electrolyte interface. The concentration polarization layer is reduced by use of a helical electrode mixer, which creates a rotational flow profile. When using the electrode in the reactor with a helical mixer, the mass transport coefficient increased by 76% in comparison with a reactor without a mixer. The conducted measurements in this study highlight the benefits that additive manufacturing brings through its ability to create geometrically complex electrode structures [32].

Heiskanen et al. conducted a simulation and theoretical study of the possibility of using L-PBF to manufacture electrochemical metal electrodes for Au recovery. The study aimed to show how this method could be used to make electrodes for recovering Au from waste. Lattice structures were used to achieve high uniform porosity and high surface area [61]. The different lattice structures were simulated to improve chlorine ($Cl_2$) gas evolution during the Au recovery. The high surface area was considered the most critical factor affecting the performance of three-dimensional electrodes in a flow reactor. Multiple minimum thickness struts were included to enable manufacture of the compact cells with L-PBF. An isotropic lattice symmetrical structure was proposed to improve electrical conductivity and electrolyte flow. A schematic of the designed electrode and a displacement plot of the simulation results are shown in **Fig. 21**.

As **Fig. 21**B shows, L-PBF can be used to fabricate this complex electrode. The use of simulation analysis demonstrated, in a proof-

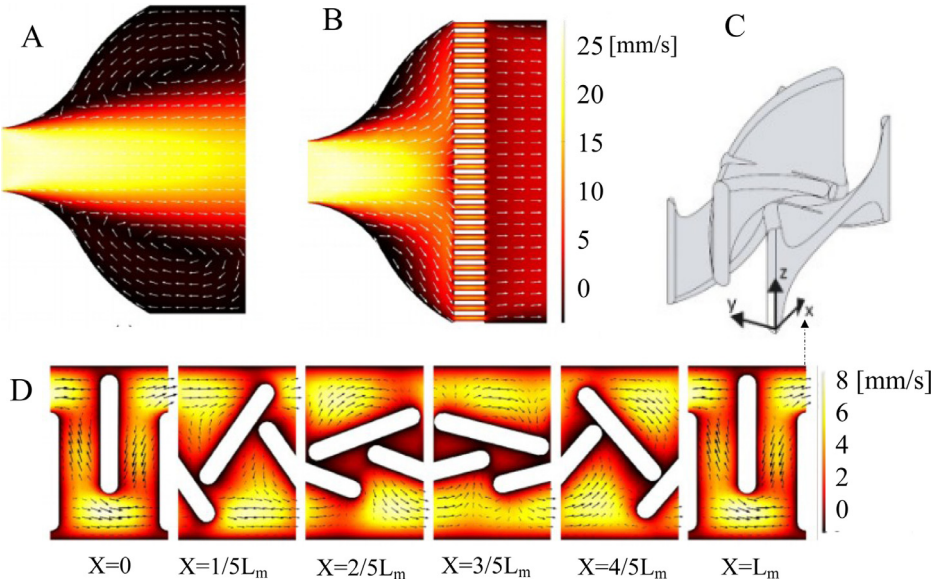


**Fig. 20.** Representation of fluid dynamic simulation of flow characteristics inside (a) the inlet without a flow distributor, (b) the inlet with a flow distributor, and the electrode mixer visualized by d) six layers along the flow path of (c) repeating unit cells and the direction of flow in the X,Y and Z axes [32]. Adapted with permission from [32]. Copyright 2017 John Wiley & Sons, Inc.

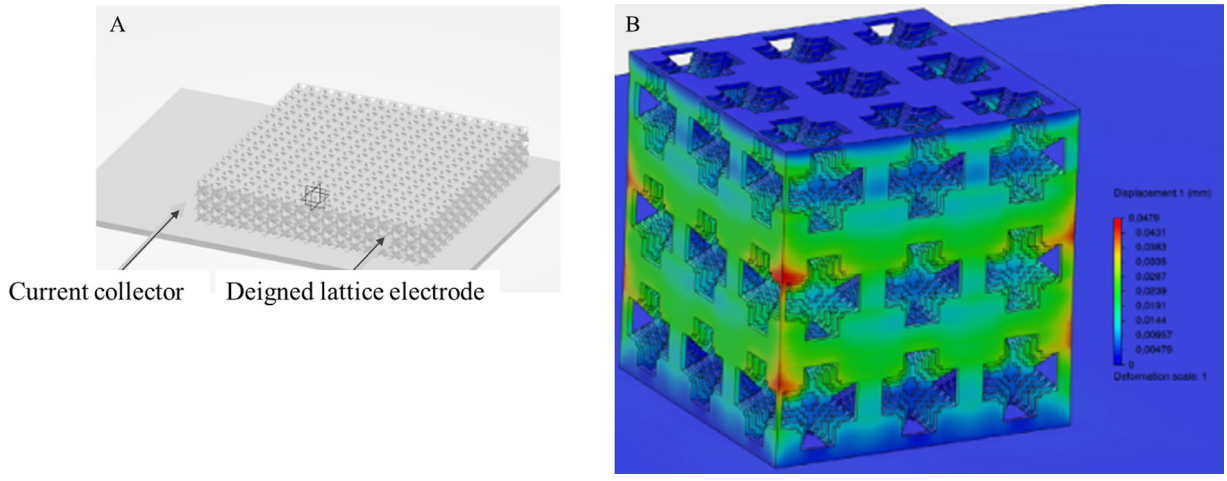


**Fig. 21.** Representation of the CAD model of an A) integrated electrode and current collector and B) a displacement plot from analysis of the simulation. Reproduced with permission from [61]. Copyright 2020 Elsevier.

of-concept, the possibility of using L-PBF for making symmetrical lattice-structured metal electrodes for Au recovery. Designing the lattice in the electrode enabled the maximum required surface area of the electrode to be achieved. The results in [39] show the potential of L-PBF for fabrication of an integrated electrode with increased surface area, enhanced isotropic porosity and uniform current distribution. These qualities can improve flow characteristics and electrical conductivity.

### *3.5. L-PBF in water splitting applications*

Ambrosi et al. conducted an experimental study to design and manufacture a solid and robust gauze-like stainless steel electrode using L-PBF on a Concept Laser machine. The electrode design was selected for higher catalytic performance due to high surface area. Functional surface modifications of the highly conductive stainless steel electrodes were required to improve the poor catalytic properties towards hydrogen and oxygen. Modification of the surface of the electrodes with either nickel (Ni), platinum (Pt) or $IrO_2$ enhanced the hydrogen evolution reaction (HER) and oxygen evolution reaction (OER). Electrodeposition of films with materials that have desirable capabilities can overcome limitations regarding the materials that can be used [7,99]. **Fig. 22** presents a sketch model, the as-built and coated electrodes.

Energy dispersive x-ray (EDX) analysis of the modified surfaces was used to study the bonding between the printed electrodes and the deposited Pt and the chemical composition. The EDX mapping showed variance in chemical presence depending on the used mode of the electrode. The modified electrodes were directly utilized in water splitting applications since the surface had been altered by electrodeposition with compounds that enhanced electrocatalytic properties towards the evolution of oxygen and hydrogen. The manufactured electrode was used in a water electrolyzer, which was tested in an alkaline solution. The results of the study showed that the as-built electrode had catalytic property, however, the reaction was weaker, and the electrode could not be used as an electrode for water splitting applications. Electrodes modified with Pt and Ti oxide ($TiO_2$) exhibited better catalytic property to HER than the Ni-modified specimen.

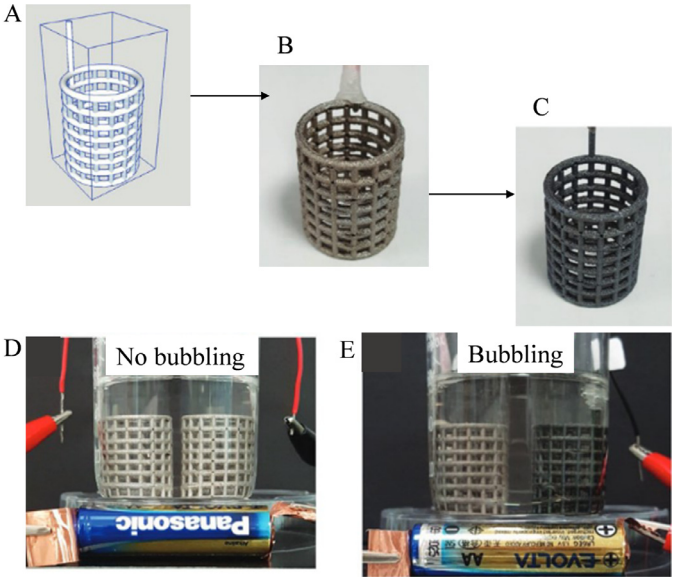


**Fig. 22.** Representation of A) the 3D model, B) as-printed stainless steel electrode, C) printed electrode with a thin layer of standard catalysts, and the experimental set up using D) the as-printed stainless steel as an anode and cathode, and E) Pt and $IrO_2$-coated gauze electrodes as a cathode and anode, respectively. Modified with permission from [7]. Copyright 2017 John Wiley & Sons, Inc.

Ambrosi et al. investigated a multi-material based electrode for water splitting. The study utilized two different AM techniques, L-PBF and material extrusion, to print a stainless steel electrode for a PLA electrolyzer cell and separators. The metal and plastic parts were printed using a Concept Laser Mlab Cusing machine and FlashForge Dreamer printer, respectively. The electrode was designed to be compatible with AM cells. The surface of the AM stainless steel electrodes was modified electrochemically to enhance performance in water splitting [48]. Fig. 23 shows a layout of the electrolyzer as used in the experiment.

The anode electrode was electrodeposited with a Ni-Fe film and the cathode with a Ni-$MoS_2$ film to improve catalytic properties. The overpotential decreased by over 250 mV compared to the plain stainless steel electrodes. The study showed the benefits of combining and integrating different AM technologies in the manufacturing process of functional devices. The study speculated that AM methods may offer a better cost structure for producing functional devices than classical methods [48].

Huang et al. conducted an experimental study with L-PBF to manufacture a 316 stainless steel electrode referred to in the study as a cellular stainless steel (CESS) electrode. The functional requirements of the designed electrode included high porosity, high specific surface area and an interconnected framework for the electrode. The main problem of metal 3D-structures manufactured with L-PBF is difficulty controlling pore distribution, size and geometry. A common consequence of this drawback is unsatisfactory mechanical properties and low electric conductivity of the finished components. Evaluation of the electrodes indicated high electronic conductivity and mechanical strength. The L-PBF CESS electrode also exhibited improved corrosion resistance when tested in an alkaline electrolyte. **Fig. 24** shows the cellular structure of the electrode designed [51].

The 3D printed structure exhibited a large electrochemical surface area and high electronic conductivity and mechanical strength. The electrocatalytic activity was also excellent for the oxygen evolution reaction [51]. 3D lattice-like metals have desirable features in water splitting applications because of their efficiency in electron, ion and bubble mitigation and high electrochemical surface

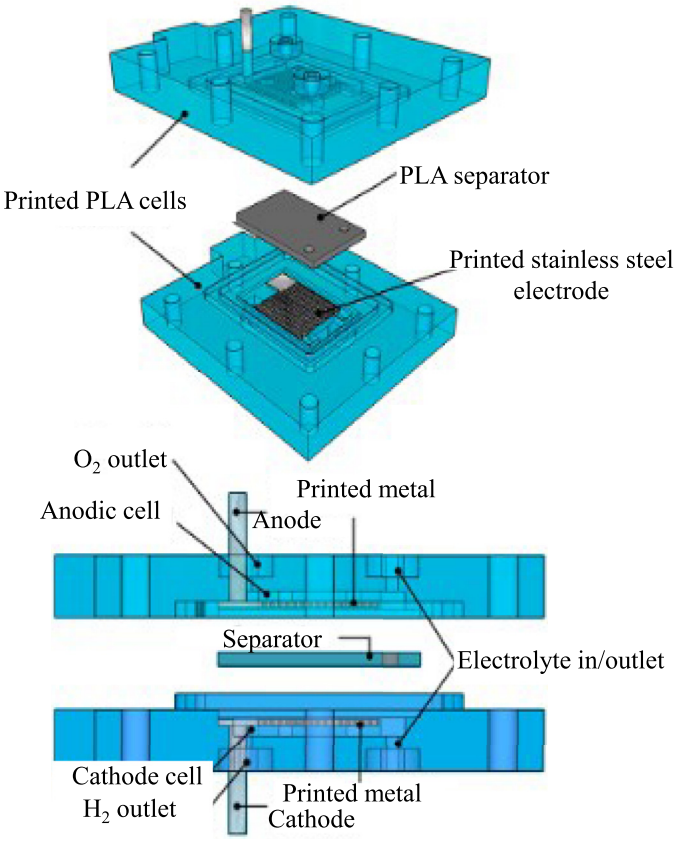


**Fig. 23.** Layout of components of the electrolyzer unit [48] Reproduced with permission from [48] Copyright (2018) American Chemical Society.

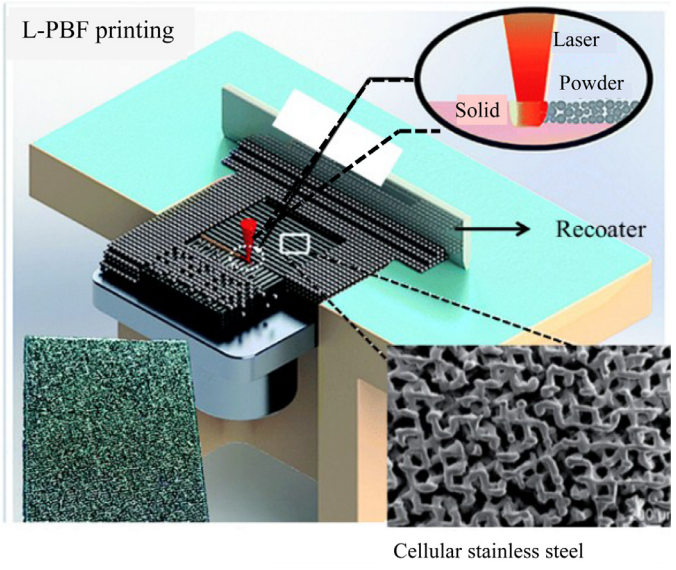


**Fig. 24.** Representation of the cellular stainless steel electrode in [51], Modified with permission from. Copyright 2017 Royal Society of Chemistry.

areas. AM can directly manufacture these metal cellular structures, thus removing constraints commonly found when manufacturing electrodes suitable for water splitting and other electrochemical applications such as REBs applications [100]. Conventionally, such foam-like metal electrodes would be manufactured with high temperature sintering. The use of L-PBF to manufacture such electrodes overcomes the poor mechanical strength, due to necking

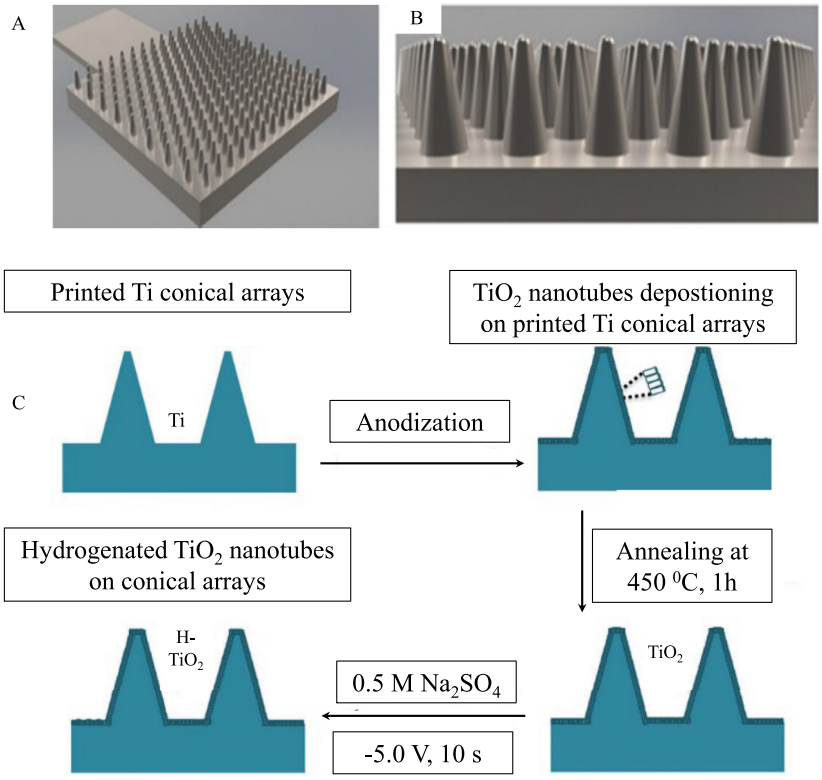


**Fig. 25.** Representation of Ti conical-arrays manufactured in [101]. A) overview, B) close-up view of conical features of the Ti electrode, and C) the surface modification procedure. Adapted with permission from [101]. Copyright 2017 John Wiley & Sons, Inc.

and the discontinuous construction, which usually characterizes foam-like electrodes produced using conventional methods.

Lee et al. performed an experimental study on Ti-based electrodes with conical arrays manufactured with L-PBF. The aim was to investigate the possibility of enhancing photoelectrochemical water splitting. The printed conical arrays increased the surface area and provided light adsorption. A Realizer SLM50 L-PBF machine was used to manufacture the Ti electrode. High surface area is a requirement for efficient photoelectrochemical water splitting because it improves charge separation and light absorption. AM enables fabrication of conical array microstructures for improved performance of the electrode. Tunable density and size are two of the main benefits that AM brings in the fabrication of micro-conical arrays. $TiO_2$ nanotubes were applied to the surfaces of the printed electrodes via electrochemical anodization for improved functionality and performance. **Fig. 25** shows the structure of the conical arrays and the surface modification procedure.

As **Fig. 25**C shows, annealing of the electrodes was done to change the amorphous phase to a crystalline phase as a way of attaining an ordered microstructure. In order to improve the electrical conductivity of the $TiO_2$, further electrochemical reduction of hydrogenated $TiO_2$ was done on the already annealed conical arrays.

### 3.6. L-PBF in REBs applications

L-PBF can be used to manufacture electrodes for REB applications using metals such as Al, Li, Na and their sulphides ($S^{2-}$) or oxides ($O^{2-}$). Carbon-based materials are required as an active or additive material for almost all existing AM electrodes used in battery applications [47,102]. Batteries may be film-based or structure-based and are used in actuator drives, biomedical sensors and micro-electro-mechanical systems.

Sun et al. reviewed the advantages of enhancing charge transport in electrochemical systems by using AM to make foam-like and ultra-thin electrodes with low mass loadings. The study showed that making electrodes weighing less than 10 mg/cm$^2$, which is not achievable with conventional methods, can improve performance and offers superior energy or power density. For example, smart micropores and complex structures suitable for improved electrochemical properties can be manufactured with L-PBF [103]. The integration of pores into battery electrodes can contribute to improved ion transport capacity by providing a continuous conductive network for electron transport and a fully interconnected hierarchical porosity [100].

Zhao et al. studied the effect of using L-PBF for the manufacture of Ti-based interlocking electrodes for supercapacitors. The electrodes were fabricated on a Realizer SLM50 metal printer. The material used in 3D printing of the electrode was Ti-6Al-4 V and both the up and down plates measured 1 cm$^2$. Each half of the electrode was designed to hold vertical pillars of 500 $\mu$m by 8 mm diameter. The top plates had 32 pillars, whereas the bottom had 32 pillars. The L-PBF manufactured electrodes offered enhanced surface area. The vertical pillar surfaces of the top electrode were plated with polypyrrole (PPy) to create an electroactive surface. The areal energy density was found to be three times higher for the PPy-coated electrode (2.98 × 10–6 Wh cm-2) than a comparable planar electrode (0.92 × 10–6 Wh cm-2). Capacitance retention of 90% and 75% was recorded for the coated electrodes, measured at a current density of 14.98 mA cm3 after 500 and 1000 cycles. About 56% capacitance retention was achieved with the improved PPy-coated Ti-6Al-4 V electrode [104]. **Fig. 26** shows the designed electrode and the approach used to electrocoat the electrode.

The active-passive state of L-PBF manufactured Al alloy ($AlSi_{12}$) electrodes on a ProX® DMP 200 machine was evaluated by Chiu et al. The study found that L-PBF manufactured $AlSi_{12}$ alloy electrodes had better passivation than conventionally cast electrodes of

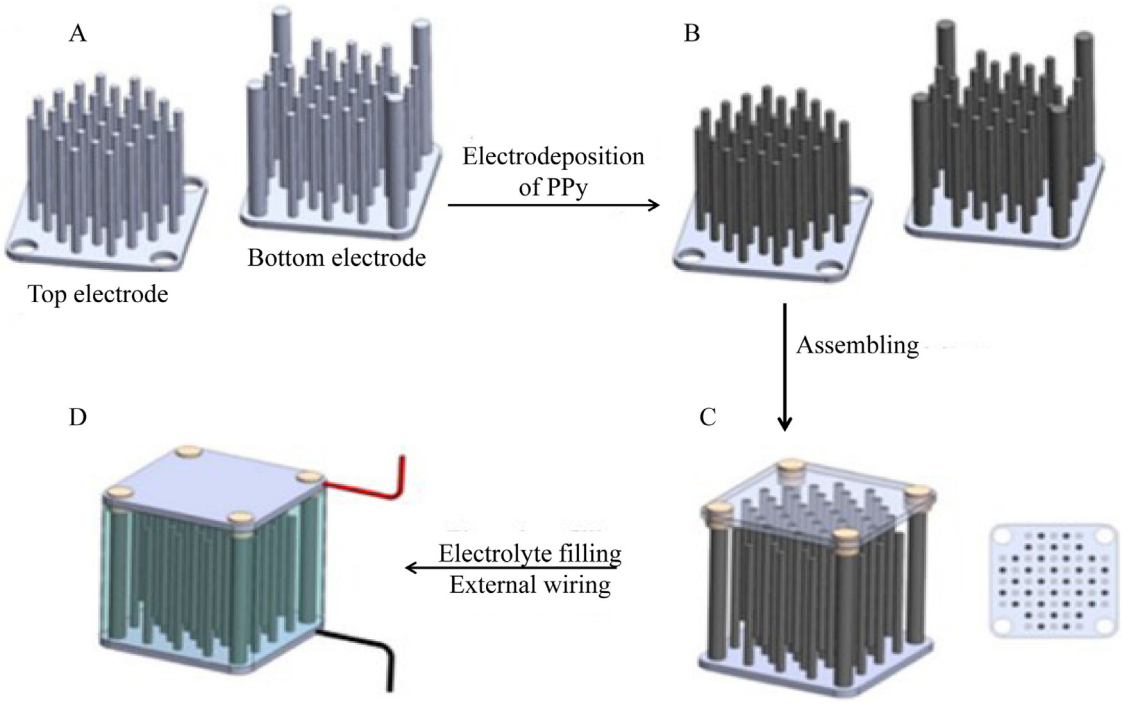


**Fig. 26.** Schematic of the A) as-printed top and bottom electrodes, B) PPy-coated electrodes, C) assembly of Ti electrodes to top and bottom plates, and D) the experimental setup. Reproduced with permission from [104]. Copyright 2020 Elsevier.

the same materials, which enhanced the corrosion behavior of the AlSi12 electrodes. The layerwise manufacturing of the electrodes improved the corrosion behavior of the L-PBF manufactured $AlSi_{12}$ alloy electrodes by enabling the incorporation of an amorphous passive layer of fine columnar Al grains in the silicon networks [105].

Jha et al. conducted experimental study to investigate the morphology impacts of L-PBF manufactured electrodes in rechargeable Li-ion batteries. The electrodes in the study were manufactured of Al alloy on a ProX DMP 200 L-PBF machine. Amorphous silicon dioxide (SiO2) nanoparticles were added as active material (with 70–90 wt.% of Al, 10–20 wt.% of Si) to the as-printed lattice structure electrodes in rechargeable Li-ion batteries. The $SiO_2$ nanoparticles were added to the as-printed lattice structure $AlSi_{12}$ as the outer layer by the Sol-Gel method to increase the charge capacity of Li-ion battery. The deposition of $SiO_2$ nanoparticles on an $AlSi_{12}$ structured composite electrode theoretically resulted in an increased surface area of the electrode. The pore sizes measured by 3DXpert manufacturing software for the small, medium, and large pore size electrodes were 2000 $\mu$m, 2500 $\mu$m, and 3000 $\mu$m, respectively. The non-coated cubic lattice structure electrode increased the non-Faradic current at the maximum voltage value in comparison to a solid electrode. The higher current can be ascribed to the greater surface area provided by the lattice structured design. In addition, the authors attributed the higher surface area indicated by the shift in the non-Faradic region to better electrolyte-electrode electrochemical reactions in the battery cell.

In addition, the electrode activated with the SiO2 nanoparticles raised the intercalation of Li ions from the electrolyte to the target electrode. The enhanced capacity in the CV curve of the LC, compared to the phase transformation characteristics of the non-porous electrode could be a result of the presence of pores. No capacity retention was observed for the electrode without active material. The non-Faradic current was minimized also by the active material (SiO2). The pore geometry, morphology, and pore distribution had an impact on the performance of the electrode by distributing active material mass. For instance, on the one hand, the 2000 $\mu$m pore electrode provides higher specific capacity than that of the 2500 $\mu$m pore electrode, whereas the 3000 $\mu$m pore electrode contrarily had the highest specific capacity. Therefore, the kinetic diffusion and ion transport from the electrolyte into the active material can be influenced by pore size and mass distribution of the active material. The presence of pores with no active material deposition (non-coated) in the cubic porous electrode raises the non-Faradic current by a factor of two (at the highest voltage value) relative to that of an electrode with no pores at all. AlSi12 composite material was introduced as an ideal choice for the 3D-printed electrode. The advantage of using L-PBF is based on the high temperature of the manufacturing process, which prevents oxidization of the electrodes. This study identified areas for future research in kinetics reactions in open-lattice hierarchically structured AM electrodes.

## 4. Results and discussions

In this study, various research papers about the utilization of L-PBF in the manufacturing of electrodes were reviewed. The research was limited to metal electrodes for use in electrochemical cells. The aim of this study was to identify the benefits and opportunities that L-PBF provides in the manufacture of components for electrochemical applications. Several of the reviewed articles are laboratory studies and do not report potential industrial benefits. Further research is thus needed to ascertain the relevance of the presented findings to commercial application.

The review shows that many different materials and alloys can potentially be printed on L-PBF machine systems. Stainless steel was found to be the most used material for electrochemical applications. This review also found that L-PBF can be used to manufacture multi-material electrodes and electrodes with various pore sizes. Many of the studies reviewed highlight utilization of L-PBF as a viable technique to manufacture intricate electrodes with optimized characteristics, for example, coarse surfaces and optimized

**Table 1**
Summary of the research case studies.

| Application | Materials and characteristic | Results | Challenges | Ref. |
|---|---|---|---|---|
| EDM tool electrode | • Bronze-nickel alloy.<br>• Pure Cupper (Cu) (□50 $\mu$m).<br>• Stainless steel alloy (DS20 (□20 $\mu$m).<br>• Mixture of 50 vol% pure Cu and 50 vol% standard EOS steel alloy.<br>• AlSi10Mg.<br>• Tungsten carbide cobalt | • A complex flush channel was designed.<br>• The bronze-nickel powder showed the best performance.<br>• Less time and costs in manufacturing. | • The electrodes did not perform as well as the comparable solid copper electrodes.<br>• Insufficient densification of the tool and wear resistance.<br>• Optimizing the process parameters to reduce the porosity of the electrodes.<br>• Controlling of *Ev* during the L-PBF may not easily be controlled with certain materials. | [50]<br>[90]<br>[20] |
| Substance detection | • Stainless steel plated with iridium oxide (IrO2) film.<br>• Stainless steel gold (Au) plated.<br>• Stainless steel coated with Bismuth (Bi).<br>• Stainless steel Au coated.<br>• Stainless steel Au plated. | • Sensitivity to phenol and p-aminophenol (p-AP) detection was obtained.<br>• Au plated electrode improved both acetaminophen and dopamine detection.<br>• The sensitivity of Au plated electrode was increased by 4.7 times. | • Stainless steel electrode is a poor material for applying in alkaline solutions.<br>• The Au -plated AM stainless steel electrode showed a weak performance for phenol. | [31]<br>[96]<br>[97]<br>[98] |
| ECM | • Powder mixture (70 wt.% alloy steel (42CrMo4).<br>• 20 wt.% Cu-Tin alloy (CuSn8), 10 wt.% Ni). | • L-PBF built lattice-like electrodes offered a vigorous flow for electrolytic fluid.<br>• Optimized lattice structures enhanced electrode performance.<br>• Electrolyte flow rate for increased machining rate were improved with optimized L-PBF electrodes | • Flow marks appeared to form on the machined surface. When the gap width was wide due to cavitation and the difference in the electrolyte flow rate.<br>• Further experimental studies on the electrolyte flow rate is needed to control the area of the lattice structure. | [49] |
| Flow reactors | • Stainless steel) Ni coated.<br>• Stainless steel (X2CrNiMo 17–12–2). | • Scaffold-like structure comparable and offered better functionality, RVS and conventional planar electrodes to improve mass transport.<br>• The surface area and porosity of the electrode were enhanced.<br>• The continuous manufactured model of the electrode and the current collector as a single metallic unit using AM controls the corrosion probability compared to the welded joints.<br>• Due to a rotational flow profile, concentration polarization effects were minimized in the transport limited reactions.<br>• The mass transport coefficient was increased by 76%.<br>• The possibility of the symmetrical lattice structured manufacturing was approved by simulation analysis. | • No experimental studies were performed to explain how the scaffold AM structure could enhance the surface area, porosity, and controlled corrosivity of the current collector and the patterned structure.<br>• The material selection as a critical item could be focused on future research. | [30]<br>[32]<br>[61] |
| Water splitting | • Stainless steel (CL 20ES) coated with Ni film.<br>• Stainless steel (CL 20ES)<br>• coated with Pt film.<br>• Stainless steel (CL 20ES)<br>• coated with IrO2 film.<br>• Stainless steel.<br>• Stainless steel coated with Ni-Fe film.<br>• Stainless steel coated with Ni-MoS2.<br>• Stainless steel (316 L stainless).<br>• Titanium (Ti), with TiO2 nanotubes. | • Micro-conical arrays Ti electrode increased anodization performance.<br>• L-PBF allowed controlling of pore distribution, sizes, and geometry than CM electrode.<br>• Improved mechanical properties with L-PBF electrodes.<br>• An L-PBF built cellular stainless steel (CESS) electrode improved corrosion resistance with electronic conductivity, and mechanical properties in an alkaline electrolyte. | • Weak catalytic property was seen in the L-PBF stainless steel electrodes. | [7]<br>[48]<br>[51]<br>[101] |
| REBs | • Ti (Ti6Al4V) coated with | • L-PBF electrodes enhanced charge | • Gap in literature on the | [100]<br>[104]<br>[105] |

shapes such as lattice zigzag configurations. The ability to design electrodes with such geometries can enable cost-effective electrochemical processing due to the enhanced efficiency of the electrodes.

One objective of this review was to ascertain the state-of-the-art of knowledge about the use of L-PBF for the manufacture of electrodes for Au recovery. However, the review, did not find existing studies that directly examine the application of L-PBF for manufacturing of metal electrodes for gold recovery in spite of many potential benefits. The only existing studies of L-PBF for Au recovery in the literature were polymer based [43,72]. A clear gap in the literature exists as regards investigation of the utilization of L-PBF for manufacturing of metal electrodes for Au recovery.

The advantages of using multi-materials for electrodes are improved functionality and reduced cost, as cheaper materials can be used as base material and coated with more expensive material. Stainless steel, for instance, can be printed in complex shapes to form the base of the electrode, which will improve mass transport properties, and can be surface modified with Au or SiO2 nanoparticles to achieve enhanced electrochemical performance. A summary of the case studies reviewed giving the results achieved and challenges encountered because of either the L-PBF process or the materials used is presented in Table 1.

## Conclusions

This study reviewed papers investigating the applicability of L-PBF to produce metal electrodes for six types of electrochemical applications, namely, electrical discharge machining (EDM), substance detection, electrochemical machining (ECM), flow reactors, water splitting and rechargeable batteries (REBs). The studies reviewed were related to utilization of AM of metal electrodes used in electrochemical processes. This study evaluated cases of L-PBF in the selected application fields in terms of design and types of metals materials for electrochemical electrodes. The study has shown that there are not many studies about the utilization of L-PBF for the manufacture of electrodes for electrochemical applications. Moreover, many of the existing studies focus on theoretical aspects, thus, more experiments are needed to assess the potential benefits of L-PBF in industrial sectors.

The review demonstrated the potential benefits of L-PBF as regards optimization of electrode shape, cost and performance. L-PBF manufacturing enables optimization of the mass transport properties of electrodes and permits design of complex geometries able to reduce flow resistance. The production of complex designs is not straightforward when using conventional methods. Component size are limited according to size of build platform. L-PBF is limited by need of support structures which can increase production cost if not well planned with the right use of simulations and DfAM guidelines.

The industrial relevance of this article is that it illustrates the potential benefits and drawbacks of using L-PBF to produce components used in electrochemical applications. The use of L-PBF will enable industries to integrate features such as lattice and tortuous structures into electrochemical equipment to produce functionally complex electrodes without increasing cost. A further benefit is that L-PBF can be used to manufacture tailored metal electrodes that can be coated with functional materials to suit specific functions. The use of L-PBF can enhance the sustainability score of industries. Lasers-driven fusion is light-based energy which are energy efficient as they do not generate greenhouse gas emissions (GHGs) [107,108] on the manufacturing phase thus has low environmental impact. Nevertheless, a comprehensive lifecycle analysis may show the electrical power and materials used in the process may contribute to GHGs by means of sources of energy and type of releases.

The main contributions of L-PBF in manufacturing of separation units for electrochemical applications are:

1 Effective application L-PBF can remove design limitations in electrode design thus improve electrode performance.
2 The use of simulation driven software can enable creation of optimized and energy-efficient electrodes for enhanced part functionality and cost-effectiveness.
3 L-PBF allows different metal powders to be combined for a single part with tailored component characteristics.
4 Functional electrochemical materials can be bonded effectively to metal AM electrodes to improve performance and cost efficacy.

Few articles can be found in literature that investigate L-PBF electrodes and almost all the studies are based on prototypes. Thus, there is insufficient data for reliable analysis to assess industrial use. Moreover, no empirical studies about Au recovery with metal-based printed electrodes have been presented. Therefore, it would be important to continue study of L-PBF and manufacture of metal-based electrodes for Au recovery.

The studies reviewed show that L-PBF manufacturing has considerable potential for the production of components used in electrochemistry and demonstrate that L-PBF can offer benefits such as improved efficiency, lower production costs, greater freedom in parts design, and enhanced parts optimization for specific applications. Further studies must consider the manufacturability and performance of electrodes for Au recovery.

## Declaration of Competing Interest

None.

## Acknowledgments

Authors would like to express their gratitude to all partners and companies of the ReGold-AM project for financial support during this study. The authors would like to thank Peter Jones for providing valuable language help and proofreading the article.

## References

[1] ISO/ASTM, ISO/ASTM 52900-2015: additive manufacturing – general principles – terminology, 2015. https://www.iso.org/obp/ui/#iso:std:iso-astm:52900:ed-1:v1:en (accessed June 5, 2020).
[2] J.C. Ferreira, A.S. Mateus, N.F. Alves, Rapid tooling aided by reverse engineering to manufacture EDM electrodes, Int. J. Adv. Manuf. Technol. 34 (2007) 1133–1143, doi:10.1007/s00170-006-0690-4.
[3] K. Plewa, 3D Print with Reverse Engineering: the Best Practices, Sculpteo, 2019 https://www.sculpteo.com/blog/2019/12/10/3d-printing-and-reverse-engineering-how-to-improve-your-production/ (accessed September 16, 2020).
[4] A.S.Ullah Tashi, A. Kubo, Geometric modeling and 3D printing using recursively generated point cloud, Math. Comput. Appl. 24 (2019) 83, doi:10.3390/mca24030083.
[5] Gibson, Powder Bed Fusion | Additive Manufacturing Research Group, Loughborough University, 2010 https://www.lboro.ac.uk/research/amrg/about/the7categoriesofadditivemanufacturing/powderbedfusion/ #:~:text=Powder bed fusion (PBF) methods,and fuse material powder together.&text=The process sinters the powder,to fuse powder material together. (accessed August 19, 2020).
[6] Y. Zhang, W. Jarosinski, Y.G. Jung, J. Zhang, Additive manufacturing processes and equipment, in: J. Zhang, Y.-G. Jung (Eds.), Additive Manufacturing Materials Processing Quantification and Applications, Elsevier, 2018, pp. 39–51, doi:10.1016/B978-0-12-812155-9.00002-5.
[7] A. Ambrosi, M. Pumera, Self-contained polymer/metal 3D printed electrochemical platform for tailored water splitting, Adv. Funct. Mater. 28 (2018) 1700655, doi:10.1002/adfm.201700655.
[8] I. Flores, N. Kretzschmar, A.H. Azman, S. Chekurov, D.B. Pedersen, A. Chaudhuri, Implications of lattice structures on economics and productivity of metal powder bed fusion, Addit. Manuf. 31 (2020) 100947, doi:10.1016/j.addma.2019.100947.
[9] T. Hupfeld, S. Salamon, J. Landers, A. Sommereyns, C. Doñate Buendia, J. Schmidt, H. Wende, M. Schmidt, S. Barcikowski, B. Gökce, 3D Printing of magnetic parts by Laser Powder Bed Fusion of iron oxide nanoparticle

functionalized polyamide powders, J. Mater. Chem. C. (2020), doi:10.1039/d0tc02740e.
[10] C. Huo, X. Tian, Y. Nan, D. Li, Hierarchically porous alumina ceramic catalyst carrier prepared by powder bed fusion, J. Eur. Ceram. Soc. 40 (2020) 4253–4264, doi:10.1016/j.jeurceramsoc.2020.03.059.
[11] R. Singh, A. Gupta, O. Tripathi, S. Srivastava, B. Singh, A. Awasthi, S.K. Rajput, P. Sonia, P. Singhal, K.K. Saxena, et al., Powder bed fusion process in additive manufacturing: an overview, in: K.K. Singh, Wadesh Kumar, Akinlabi, Esther Titilayo, Kaushik Kumar, Davim, J. Paulo, et al. (Eds.), Materials Today Proc, Elsevier Ltd, 2019, pp. 3058–3070, doi:10.1016/j.matpr.2020.02.635.
[12] M.G. Moleirinho, S. Feast, A.S. Moreira, R.J.S. Silva, P.M. Alves, M.J.T. Carrondo, T. Huber, C. Fee, C. Peixoto, 3D-printed ordered bed structures for chromatographic purification of enveloped and non-enveloped viral particles, Sep. Purif. Technol. 254 (2021) 1383–5866, doi:10.1016/j.seppur.2020.117681.
[13] K. Akshay Kumar, K. Ghosh, O. Alduhaish, M. Pumera, Metal-plated 3D-printed electrode for electrochemical detection of carbohydrates, Electrochem. Commun. 120 (2020) 106827, doi:10.1016/j.elecom.2020.106827.
[14] I. Campbell, D. Bourell, 3D printing and additive manufacturing global state of the industry, Colorado, 2020.
[15] SculpteoThe State of 3D Printing Report: 2020, Sculpteo, 2020 by https://www.sculpteo.com/en/ebooks/state-of-3d-printing-report-2020/ (accessed June 5, 2020).
[16] V. Urlea, V. Brailovski, Electropolishing and electropolishing-related allowances for powder bed selectively laser-melted Ti-6Al-4V alloy components, J. Mater. Process. Technol. 242 (2017) 1–11, doi:10.1016/j.jmatprotec.2016.11.014.
[17] A.E.O. Daraban, C.S. Negrea, F.G.P. Artimon, D. Angelescu, G. Popan, S.I. Gheorghe, M. Gheorghe, A deep look at metal additive manufacturing recycling and use tools for sustainability performance, Sustain 11 (2019) 5494, doi:10.3390/su11195494.
[18] M. Mani, K.W. Lyons, S.K. Gupta, Sustainability characterization for additive manufacturing, J. Res. Natl. Inst. Stand. Technol. 119 (2014) 419–428, doi:10.6028/jres.119.016.
[19] C. Wei, Z. Zhang, D. Cheng, Z. Sun, M. Zhu, L. Li, An overview of laser-based multiple metallic material additive manufacturing: from macro: from micro-scales, Int. J. Extrem. Manuf. (2021), doi:10.1088/2631-7990/abce04.
[20] E. Uhlmann, A. Bergmann, R. Bolz, W. Gridin, Application of additive manufactured tungsten carbide tool electrodes in EDM, in: Procedia CIRP, Elsevier B.V., 2018, pp. 86–90, doi:10.1016/j.procir.2017.12.027.
[21] R. Tino, M. Leary, A. Yeo, E. Kyriakou, T. Kron, M. Brandt, Additive manufacturing in radiation oncology: a review of clinical practice, emerging trends and research opportunities, Int. J. Extrem. Manuf. (2020), doi:10.1088/2631-7990/ab70af.
[22] A. Huckstepp, Powder bed fusion (PBF), Digit. Alloy. Guid. to Met. Addit. Manuf. (2019) https://www.digitalalloys.com/blog/powder-bed-fusion/. (accessed November 20, 2020).
[23] P. Morrow, The Value of Design for Additive Manufacturing (DFAM) : Additive Manufacturing Magazine, Gardner Bus. Media, Inc, 2020 https://www.additivemanufacturing.media/blog/post/the-value-of-design-for-additive-manufacturing-dfam (accessed November 20, 2020).
[24] M. Alghamdy, R. Ahmad, B. Alsayyed, Material selection methodology for additive manufacturing applications, in: Procedia CIRP, Elsevier B.V., 2019, pp. 486–490, doi:10.1016/j.procir.2019.04.265.
[25] A.A. Zadpoor, J. Malda, Additive manufacturing of biomaterials, tissues, and organs, Ann. Biomed. Eng. (2017) 45, doi:10.1007/s10439-016-1719-y.
[26] P. Saxena, M. Papanikolaou, E. Pagone, K. Salonitis, M. Jolly, Digital manufacturing for foundries 4.0, in: A Tomsett (Ed.), Light Metals 2020. Minerals Metals and Materials Series, Springer, Cham, 2020 https://doi-org.ezproxy.cc.lut.fi/10.1007/978-3-030-36408-3_138 (accessed October 29, 2020).
[27] Delva, Hybrid printing is a cost-effective way to improve production efficiency, (2020). https://delva.fi/en/news/hybrid-printing-is-a-cost-effective-way-to-improve-production-efficiency/ (accessed November 4, 2020).
[28] SHINING 3DMetal 3D Printing Promotes Revolution in Valve Design and Manufacturing, SHINING 3D, 2020 https://www.shining3d.com/blog/metal-3d-printing-promotes-revolution-in-valve-design-and-manufacturing/ (accessed October 26, 2020).
[29] A. del Puerto, Future sustainability and the socioeconomic dimension of digital fabrication, in: Sustainable Innovation Conference 2015, Surrey, 2015, pp. 1–13. https://www.academia.edu/19643439/Future_sustainability_and_the_socioeconomic_dimension_of_digital_fabrication.
[30] L.F. Arenas, C. Ponce de León, F.C. Walsh, 3D-printed porous electrodes for advanced electrochemical flow reactors: a Ni/stainless steel electrode and its mass transport characteristics, Electrochem. Commun. 77 (2017) 133–137, doi:10.1016/j.elecom.2017.03.009.
[31] A. Ambrosi, J.G.S. Moo, M. Pumera, Helical 3D-printed metal electrodes as custom-shaped 3D platform for electrochemical devices, Adv. Funct. Mater. 26 (2016) 698–703, doi:10.1002/adfm.201503902.
[32] J. Lölsberg, O. Starck, S. Stiefel, J. Hereijgers, T. Breugelmans, M. Wessling, 3D-printed electrodes with improved mass transport properties, ChemElectroChem. 4 (2017) 3309–3313, doi:10.1002/celc.201700662.
[33] M.P. Browne, F. Novotný, Z. Sofer, M. Pumera, 3D printed graphene electrodes' electrochemical activation, ACS Appl. Mater. Interfaces 10 (2018) 40294–40301, doi:10.1021/acsami.8b14701.
[34] S. Ganesh Sarvankar, S.N. Yewale, Additive manufacturing in automobile industry, IJRAME Publ 7 (2019) 1–10.
[35] H. Torbati-Sarraf, I. Ghamarian, B. Poorganji, S.A. Torbati-Sarraf, An Investigation on the role of crystallographic texture on anisotropic electrochemical behavior of a commercially pure nickel manufactured by laser powder bed fusion (L-PBF) additive manufacturing, Electrochim. Acta. 354 (2020) 136694, doi:10.1016/j.electacta.2020.136694.
[36] C. Vyas, G. Poologasundarampillai, J. Hoyland, P. Bartolo, 3D printing of biocomposites for osteochondral tissue engineering, in: Biomedical Composition, Elsevier, 2017, pp. 261–302, doi:10.1016/b978-0-08-100752-5.00013-5.
[37] A. Younis, D. Chu, S. Li, Electrochemical processes in manufacturing, in: Handbook of Manufacturing Engineering and Technology, Springer, London, 2015, pp. 2851–2889, doi:10.1007/978-1-4471-4670-4_32.
[38] B. Li, D. Xia, Anionic Redox in Rechargeable Lithium Batteries, Adv. Mater. (2017) 29, doi:10.1002/adma.201701054.
[39] M. Rosenbaum, F. Aulenta, M. Villano, L.T. Angenent, Cathodes as electron donors for microbial metabolism: which extracellular electron transfer mechanisms are involved? Bioresour. Technol. 102 (2011) 324–333, doi:10.1016/j.biortech.2010.07.008.
[40] G. Inzelt, A. Lewenstam, F. Scholz, Handbook of Reference Electrodes, Springer, Berlin Heidelberg, 2013, doi:10.1007/978-3-642-36188-3.
[41] S.C. Perry, C. Ponce de León, F.C. Walsh, Review—The Design, performance and continuing development of electrochemical reactors for clean electrosynthesis, J. Electrochem. Soc. (2020) 167, doi:10.1149/1945-7111/abc58e.
[42] F. Ali, M. Gohar, I. Khan, MHD flow of water-based Brinkman type nanofluid over a vertical plate embedded in a porous medium with variable surface velocity, temperature and concentration, J. Mol. Liq. 233 (2016) 412–419, doi:10.1016/j.molliq.2016.08.068.
[43] N.A. Mohd Zin, I. Khan, S. Shafie, The impact silver nanoparticles on MHD free convection flow of Jeffrey fluid over an oscillating vertical plate embedded in a porous medium, J. Mol. Liq. 222 (2016) 138–150, doi:10.1016/j.molliq.2016.06.098.
[44] A. Hussanan, Z. Ismail, I. Khan, A.G. Hussein, S. Shafie, Unsteady boundary layer MHD free convection flow in a porous medium with constant mass diffusion and Newtonian heating, Eur. Phys. J. Plus. 129 (2014) 46, doi:10.1140/epjp/i2014-14046-x.
[45] N.A. Sheikh, F. Ali, M. Saqib, I. Khan, S.A.A. Jan, A comparative study of Atangana-Baleanu and Caputo-Fabrizio fractional derivatives to the convective flow of a generalized Casson fluid, Eur. Phys. J. Plus. 132 (2017) 1–14, doi:10.1140/epjp/i2017-11326-y.
[46] N.A. Sheikh, F. Ali, M. Saqib, I. Khan, S.A.A. Jan, A.S. Alshomrani, M.S. Alghamdi, Comparison and analysis of the Atangana–Baleanu and Caputo–Fabrizio fractional derivatives for generalized Casson fluid model with heat generation and chemical reaction, Results Phys 7 (2017) 789–800, doi:10.1016/j.rinp.2017.01.025.
[47] M. Zhang, H. Mei, P. Chang, L. Cheng, 3D printing of structured electrodes for rechargeable batteries, J. Mater. Chem. A. 8 (2020) 10670–10694, doi:10.1039/d0ta02099k.
[48] A. Ambrosi, M. Pumera, Multimaterial 3D-printed water electrolyzer with earth-abundant electrodeposited catalysts, ACS Sustain. Chem. Eng. 6 (2018) 16968–16975, doi:10.1021/acssuschemeng.8b04327.
[49] T. Koyano, A. Hosokawa, R. Igusa, T. Ueda, Electrochemical machining using porous electrodes fabricated by powder bed fusion additive manufacturing process, CIRP Ann. - Manuf. Technol. 66 (2017) 213–216, doi:10.1016/j.cirp.2017.04.127.
[50] F.L. Amorim, A. Lohrengel, N. Müller, G. Schäfer, T. Czelusniak, Performance of sinking EDM electrodes made by selective laser sintering technique, Int. J. Adv. Manuf. Technol. 65 (2013) 1423–1428, doi:10.1007/s00170-012-4267-0.
[51] X. Huang, S. Chang, W.S.V. Lee, J. Ding, J.M. Xue, Three-dimensional printed cellular stainless steel as a high-activity catalytic electrode for oxygen evolution, J. Mater. Chem. A. 5 (2017) 18176–18182, doi:10.1039/c7ta03023a.
[52] M. Aysha, The List of Bicycles Made with 3D Printing Technologies, 3Dnatives, 3D Nativ, 2020 https://www.3dnatives.com/en/ranking-3d-printed-bikes-220920204/#! (accessed September 22, 2020).
[53] I. Gibson, D.W. Rosen, B. Stucker, Additive manufacturing technologies: rapid prototyping to direct digital manufacturing, 2010. https://doi.org/10.1007/978-1-4419-1120-9.
[54] J. Waller, Qualification & certification of additively manufactured parts for NASA applications, NASA Saf. Cent. Webinar. (2019) https://ntrs.nasa.gov/search.jsp?R=20190000354. (accessed June 1, 2020).
[55] AutodeskMechanical Engineer's Guide to Lightweighting, eBook, 2019 https://www.autodesk.com/industry/manufacturing/resources/mechanical-engineer/lightweighting-guide (accessed July 21, 2020).
[56] O.D. Neikov, Powders for additive manufacturing processing, in: O.D. Neikov, N.V. Yefimov NaboychenkoStanislav (Eds.), Handbook Non-Ferrous Metals Powders, 2nd Ed., Elsevier, Amsterdam, Netherlands, 2019, pp. 373–399, doi:10.1016/b978-0-08-100543-9.00013-0.
[57] J. Marschewski, S. Jung, P. Ruch, N. Prasad, S. Mazzotti, B. Michel, D. Poulikakos, Mixing with herringbone-inspired microstructures: overcoming the diffusion limit in co-laminar microfluidic devices, Lab Chip 15 (2015) 1923–1933, doi:10.1039/c5lc00045a.
[58] J. Hereijgers, J. Schalck, T. Breugelmans, Mass transfer and hydrodynamic characterization of structured 3D electrodes for electrochemistry, Chem. Eng. J. 384 (2020) 123283, doi:10.1016/j.cej.2019.123283.

[59] M. Fadel, J.V. Daurelle, V. Fourmond, J. Vicente, A new electrochemical cell with a uniformly accessible electrode to study fast catalytic reactions, Phys. Chem. Chem. Phys. 21 (2019) 12360–12371, doi:10.1039/c9cp01487j.

[60] J. Tiainen, A. Grönman, A. Jaatinen-Värri, J. Backman, Flow control methods and their applicability in low-reynolds-number centrifugal compressors - a review, Int. J. Turbomach., Propuls. Power. 3 (2018) 2, doi:10.3390/ijtpp3010002.

[61] A. Heiskanen, E. Repo, H. Piili, Design of electrode for electrochemical gold separation process manufactured via laser-based powder bed fusion, Procedia CIRP 94 (2020) 383–387, doi:10.1016/j.procir.2020.09.150.

[62] E. Durham, Carnegie Mellon University –3D printing the next generation of batteries, Addit. Manuf. (AM) (2018) https://additivemanufacturing.com/2018/08/22/carnegie-mellon-university-3d-printing-the-next-generation-of-batteries/. (accessed August 19, 2020).

[63] M.F. Ashby, The properties of foams and lattices, Philos. Trans. R. Soc. A Math. Phys. Eng. Sci. 364 (2006) 15–30, doi:10.1098/rsta.2005.1678.

[64] Croft Additive ManufacturingAM Applications | Additive Manufacturing Applications | Croft AM | Croft Additive Manufacturing | | Additive Manufacturing | 3D Printing | Croft AM |Croft Additive Manufacturing, August 5, 2020 (n.d.) https://www.croftam.co.uk/designing-to-add-value/ (accessed.

[65] Etteplan, 3D Printing Case for John Deere's Hydraulic Block, Etteplan, 2020 https://www.etteplan.com/references/additive-manufacturing-design-case-john-deeres-hydraulic-block (accessed October 24, 2020).

[66] T. English, What is finite element analysis and how does it work? Interes. Eng. (2019) https://interestingengineering.com/what-is-finite-element-analysis-and-how-does-it-work#:~:text=Finite. Element Analysis or FEA,a variety of other disciplines(accessed October 24, 2020).

[67] Dazztech SolutionsDAZZTECH - CAE/Design Optimization Solutions - Image to 3D Model Processing & Visualisation, Simpleware, 2020 http://www.dazztech.com/image-to-3d-model-processing-visualisation-simpleware.html (accessed October 26, 2020).

[68] Product Research and Engineering SLAdvantages of CFD | FEA Services and Consultancy, CFD and FEA company, 2020 http://www.pretechnologies.com/services/computational-fluid-dynamics/advantage (accessed October 24, 2020).

[69] S. Hällgren, L. Pejryd, J. Ekengren, (Re)design for additive manufacturing, in: Procedia CIRP, Elsevier B.V., 2016, pp. 246–251, doi:10.1016/j.procir.2016.04.150.

[70] M. Mazur, M. Leary, S. Sun, M. Vcelka, D. Shidid, M. Brandt, Deformation and failure behaviour of Ti-6Al-4V lattice structures manufactured by selective laser melting (SLM), Int. J. Adv. Manuf. Technol. 84 (2016) 1391–1411, doi:10.1007/s00170-015-7655-4.

[71] E. Lahtinen, L. Kivijärvi, R. Tatikonda, A. Väisänen, K. Rissanen, M. Haukka, Selective recovery of gold from electronic waste using 3D-printed scavenger, ACS Omega 2 (2017) 7299–7304, doi:10.1021/acsomega.7b01215.

[72] S. Liu, Y.C. Shin, Additive manufacturing of Ti6Al4V alloy: a review, Mater. Des. 164 (2019) 107552, doi:10.1016/j.matdes.2018.107552.

[73] D. Mahmoud, M.A. Elbestawi, Selective laser melting of porosity graded lattice structures for bone implants, Int. J. Adv. Manuf. Technol. 100 (2019) 2915–2927, doi:10.1007/s00170-018-2886-9.

[74] L. Yuan, S. Ding, C. Wen, Additive manufacturing technology for porous metal implant applications and triple minimal surface structures: a review, Bioact. Mater. 4 (2019) 56–70, doi:10.1016/j.bioactmat.2018.12.003.

[75] M.S. Saleh, J. Li, J. Park, R. Panat, 3D printed hierarchically-porous microlattice electrode materials for exceptionally high specific capacity and areal capacity lithium ion batteries, Addit. Manuf. 23 (2018) 70–78, doi:10.1016/j.addma.2018.07.006.

[76] B. Rehm, D. Consultant, A. Haghshenas, A.S. Paknejad, J. Schubert, Situational problems in MPD, in: Managed Pressure Drilling, Elsevier, 2008, pp. 39–80, doi:10.1016/b978-1-933762-24-1.50008-5.

[77] H. Belyadi, E. Fathi, F. Belyadi, Hydraulic fracturing chemical selection and design, in: Hydraulic Fracturing in Unconventional Reservoirs, Elsevier, 2017, pp. 107–120, doi:10.1016/b978-0-12-849871-2.00008-3.

[78] E.S. Menon, Transmission Pipeline Calculations and Simulations Manual, Elsevier Inc., 2015, doi:10.1016/C2009-0-60912-0.

[79] R.S. Subramanian, Reynolds Number, New York, n.d. moz-extension://b538a8e2-08a1-492e-87ad-87d07582bd06/enhanced-reader.html?openApp&pdf=https%3A%2F%2Fweb2.clarkson.edu%2Fprojects%2Fsubramanian%2Fch330%2Fnotes%2FReynolds%2520Number.pdf.2020.

[80] X. Yuan, Z. Tao, H. Li, Y. Tian, Experimental investigation of surface roughness effects on flow behavior and heat transfer characteristics for circular microchannels, Chin. J. Aeronaut. 29 (2016) 1575–1581, doi:10.1016/j.cja.2016.10.006.

[81] S.G. Kandlikar, D. Schmitt, A.L. Carrano, J.B. Taylor, Characterization of surface roughness effects on pressure drop in single-phase flow in minichannels, Phys. Fluids. 17 (2005), doi:10.1063/1.1896985.

[82] A. de Vries, 3D-printed metal flow reactors and mixers, RSC Symposium 2017 Chemspec, Tomorrow's Chemistry Today, 2017 www.innosyn.com.

[83] L. Skyward, 3D Modeling and Reverse Engineering, Skyward, Ltd., 2020 (n.d.) http://skywardltd.com/index.php?id=41 (accessed October 21.

[84] T. Czelusniak, F.L. Amorim, C.F. Higa, A. Lohrengel, Development and application of new composite materials as EDM electrodes manufactured via selective laser sintering, Int. J. Adv. Manuf. Technol. 72 (2014) 1503–1512, doi:10.1007/s00170-014-5765-z.

[85] X. Sun, H. Lin, C. Zhang, X. Huang, J. Jin, S. Di, Electrosynthesized nanostructured polypyrrole on selective laser melted titanium scaffold, Surf. Coat. Technol. 370 (2019) 11–17, doi:10.1016/j.surfcoat.2019.04.078.

[86] J. Weber, A.J. Wain, H. Piili, V.P. Matilainen, A. Vuorema, G.A. Attard, F. Marken, Residual porosity of 3D-LAM-printed stainless-steel electrodes allows galvanic exchange platinisation, ChemElectroChem. 3 (2016) 1020–1025, doi:10.1002/celc.201600098.

[87] C.Y. Foo, H.N. Lim, M.A. Mahdi, M.H. Wahid, N.M. Huang, Three-dimensional printed electrode and its novel applications in electronic devices, Sci. Rep. 8 (2018) 7399, doi:10.1038/s41598-018-25861-3.

[88] J. Muñoz, M. Pumera, Accounts in 3D-printed electrochemical sensors: towards monitoring of environmental pollutants, ChemElectroChem 7 (2020) 3404–3413, doi:10.1002/celc.202000601.

[89] S. Kakooei, M.C. Ismail, B.A. Wahjoedi, Electrochemical study of iridium oxide coating on stainless steel substrate, Int. J. Electrochem. Sci. 8 (2013) 3290–3301 www.electrochemsci.org.

[90] A.K. Sahu, S.S. Mahapatra, Performance analysis of tool electrode prepared through laser sintering process during electrical discharge machining of titanium, Int. J. Adv. Manuf. Technol. 106 (2020) 1017–1041, doi:10.1007/s00170-019-04675-1.

[91] Nanopartikel.info, Tungsten carbide-cobalt _ knowledge base nanomaterials, (n.d.). https://www.nanopartikel.info/en/nanoinfo/materials/tungsten-carbide-cobalt/material-information (accessed December 1, 2020).

[92] WIELAND-WERKE AG, Semi-finished products in copper materials – basic elements of modern information technology, (n.d.). https://www.wieland.com/files/wieland/brochures/ex/semi-finished_products_high_frequency_technology_EN.pdf (accessed December 1, 2020).

[93] EGM Group, Cu-ETP technical sheet, (2020). https://www.egmgroup.it/pdfs/egm_Cu-ETP_ETP_en.pdf (accessed December 1, 2020).

[94] IBIDEN Fine Graphite Material, Ibiden fine graphite material, (2020). https://www.fgm.ibiden.co.jp/multilanguage/german-ex-75.html (accessed December 1, 2020).

[95] Ceratizits A., Ceratizit \ Carbide grades for all requirements & price categories, (n.d.). https://www.ceratizit.com/en/products/rods-preforms/carbide-grades/ (accessed November 29, 2020).

[96] T.S. Cheng, M.Z.M. Nasir, A. Ambrosi, M. Pumera, 3D-printed metal electrodes for electrochemical detection of phenols, Appl. Mater. Today. 9 (2017) 212–219, doi:10.1016/j.apmt.2017.07.005.

[97] K.Y. Lee, A. Ambrosi, M. Pumera, 3D-printed metal electrodes for heavy metals detection by anodic stripping voltammetry, Electroanalysis 29 (2017) 2444–2453, doi:10.1002/elan.201700388.

[98] B.R. Liyarita, A. Ambrosi, M. Pumera, 3D-printed electrodes for sensing of biologically active molecules, Electroanalysis 30 (2018) 1319–1326, doi:10.1002/elan.201700828.

[99] G. Caputo, I. Balog, A. Giaconia, S. Sau, A. Pozio, Experimental study for Hlx concentration by electro-electrodialysis (EED) cells in the water splitting sulfur-iodine thermochemical cycle, Chem. Eng. 3 (2019) 50, doi:10.3390/chemengineering3020050.

[100] H. Sun, J. Zhu, D. Baumann, L. Peng, Y. Xu, I. Shakir, Y. Huang, X. Duan, Hierarchical 3D electrodes for electrochemical energy storage, Nat. Rev. Mater. 4 (2019) 45–60, doi:10.1038/s41578-018-0069-9.

[101] C.Y. Lee, A.C. Taylor, S. Beirne, G.G. Wallace, 3D-printed conical arrays of $TiO_2$ electrodes for enhanced photoelectrochemical water splitting, Adv. Energy Mater. 7 (2017) 1701060, doi:10.1002/aenm.201701060.

[102] M. Kazazi, P. Abdollahi, M. Mirzaei-Moghadam, High surface area TiO2 nanospheres as a high-rate anode material for aqueous aluminium-ion batteries, Solid State Ionics 300 (2017) 32–37, doi:10.1016/j.ssi.2016.11.028.

[103] J. Li, M.C. Leu, R. Panat, J. Park, A hybrid three-dimensionally structured electrode for lithium-ion batteries via 3D printing, Mater. Des. 119 (2017) 417–424, doi:10.1016/j.matdes.2017.01.088.

[104] C. Zhao, C. Wang, R. Gorkin, S. Beirne, K. Shu, G.G. Wallace, Three dimensional (3D) printed electrodes for interdigitated supercapacitors, Electrochem. Commun. 41 (2014) 20–23, doi:10.1016/j.elecom.2014.01.013.

[105] T.M. Chiu, C. Zhang, D. Zhao, D. Yadav, K.Y. Xie, A. Elwany, H. Castaneda, Interface stability of laser powder-bed-fused AlSi12 under simulated atmospheric conditions, Corros. Sci. (2020) 175, doi:10.1016/j.corsci.2020.108861.

[106] S. Jha, Y. Chen, B. Zhang, A. Elwany, D. Parkinson, H. Liang, Influence of morphology on electrochemical and capacity performance of open-porous structured electrodes, J. Appl. Electrochem. 50 (2020) 231–244, doi:10.1007/s10800-019-01378-z.

[107] M. Bähren, A. Bauer, J.V. Bebber, J. Cochard, High-tech PHOTONICS solutions to protect the environment and preserve resources - Google Search, (2020). https://www.photonics21.org/download/ppp-services/photonics-downloads/Study_GreenPhotonics_2020_final.pdf (accessed December 1, 2020).

[108] UK Research and Innovation, Lasers and energy, (n.d.). https://stfc.ukri.org/research/lasers-and-plasma-physics/lasers-and-stfc/lasers-and-energy/ (accessed December 1, 2020).